Master of Science Thesis

Wake control using rotor tilting

Optimizing wind farm energy production through vertical wake deflection

R.M. Storm

April 4, 2018

DCSC

TU Delft

Delft Center for Systems and Control

Delft University of Technology

Wake control using rotor tilting

Optimizing wind farm energy production through vertical wake deflection

Master of Science Thesis

For obtaining the degree of Master of Science in Mechanical Engineering at Delft University of Technology

R.M. Storm

April 4, 2018

Faculty of Mechanical, Maritime and Materials Engineering · Delft University of Technology

The picture on the title page shows the normally invisible wind wakes. Due to atmospheric conditions they take shape in the clouds behind turbines in the Horns Rev offshore wind farm west of Denmark (Credit: Christian Steiness).

Delft University of Technology

Delft University Of Technology
Delft Center for Systems and Control

The undersigned hereby certify that they have read and recommend to the Faculty of Mechanical, Maritime and Materials Engineering for acceptance a thesis entitled **"Wake control using rotor tilting"** by **R.M. Storm** in partial fulfillment of the requirements for the degree of **Master of Science**.

Dated: April 4, 2018

Supervisor:

ir. B.M. Doekemeijer

Readers:

prof. dr. ir. J.W. van Wingerden

dr. ir. W.A.A.M. Bierbooms

ir. T.J. Berdowski

Abstract

Currently there is strong interest in the deployment of renewable energy sources such as wind, solar and hydro energy. This is driven in part due to the negative consequences of burning fossil fuels, such as health issues and climate change. To optimize the energy extracted in a wind farm the turbines require some control algorithm. Today, wind turbines that are part of a wind farm do not take neighbouring turbines into account when determining their control settings. This results in greedy control, where each turbine tries to align itself with the dominant wind direction and optimize its energy production using generator torque control and pitch control. During operation, each turbine creates a volume of slow-moving turbulent air behind its rotor, which is called a wake.

The issue with greedy control is that a turbine does not take into account where its wake will end up with respect to downwind turbines. By misaligning a turbine with the wind direction its trust can displace the wake. This will cause an efficiency loss on the misaligned turbine, but it can be used to increase the efficiency of a downwind turbine, leading to an increase in net power production. We know that a controller that uses yaw optimization can optimize the power production in a small scale experimental setup [Campagnolo et al., 2016]. In this particular research a line of three turbines produced 15% extra power compared to greedy control.

Wake redirection can be thought of as an attempt to efficiently mix the slower moving air in the wake with the faster stream surrounding it. This allows more of the total energy in the free stream to be extracted by any given wind farm. Yaw redirection has the potential to mix in the high velocity air that could otherwise pass through the empty space between the turbines. Tilt redirection has the potential to more efficiently mix the high velocity air that would otherwise pass over the wind farm into the air that hits the rotors [Annoni et al., 2017]. This work focuses on the development and implementation of a wake model that can be used to predict the effects of rotor tilting on the wake.

We started with the FLOw Redirection and Induction in Steady state (FLORIS) model as described in [Gebraad et al., 2014]. This model can be used to estimate the power production of a wind farm. It models the wake intensity and position and combines wakes when they overlap. The power production and wake characteristics of each turbine are predicted using

three sub-models. There is one model for the wake intensity and its velocity profile, one to estimate wake deflection and one to determine how wakes are added to each other.

In current practice, the wake deflection is modeled only in a horizontal plane, it can be driven by rotor yaw. In this work, the deflection model will be extended in such a way that the effects of rotor tilting on the wake position can be modeled.

Tuning a reduced order model such as FLORIS is notoriously difficult. In the FLORIS model, as described in [Gebraad et al., 2014] there are twelve hand tuned parameters. An important part of this research was attempting to simplify the tuning problem by making a robust parameter tuning procedure. A sensitivity analysis of the tuning parameters on the predicted power signals by FLORIS was performed. This analysis was used to identify situations where a subset of the model parameters is responsible for the variance in the predicted power production. Such situations with specific sensitivity were identified, but I lacked time and resources to fully leverage these and accurately tune the tilt extended model.

We stuck with the original nominal parameters of the different parts constituting FLORIS to conduct a case study. The case study compared predicted power increases by FLORIS with high fidelity simulations in two different Large Eddy Simulation (LES) packages. The case study was conducted by trying to optimize the power production of a small wind farm containing six turbines. The wind turbines were positioned in a two by three grid and the wind direction was aligned along the three turbines. The FLORIS model was used to optimize the yaw angles, tilt angles and both of them simultaneously for this layout. This led to four sets of control settings, the baseline case with greedy control and three optimized sets.

We found that the FLORIS model strongly overestimated the power gain caused by turbine tilt. The main reason for this over-estimation seems to be that FLORIS currently has no implementation of the ground. In effect, the wakes in FLORIS can simply disappear into the ground. The case where only the yaw angles are optimized matched the high fidelity simulations to a higher degree confirming the work done in [Bastankhah and Porté-Agel, 2016].

In conclusion, tilt control seems to have the potential to extract more energy from a certain atmospheric region. This is postulated because the air that gets forced on to rotors using tilt control would otherwise have passed unused over a wind farm. However, the model proposed in this thesis is insufficient to analyze the possible energy gains because it overestimates the effect of turbine tilting. This biggest problem with the FLORIS model is that it lacks a method for modeling the interaction between the ground and a wake. For future research the main priority should be implementing a solution to that problem.

Acknowledgements

I would like to thank my day to day supervisor ir. B.M. Doekemeijer and prof. dr. ir. J.W. van Wingerden for their assistance during the writing of this thesis. I would also like to thank them and the people at National Renewable Energy Laboratory for the opportunity to spend two months at the National Wind Technology Center in Boulder, Colorado. Special thanks go out to Paul A.Fleming and Jennifer Annoni for hosting me during my stay. I would also like to thank my friends and family for their support and company during this thesis work. And most of all I want to thank Astrid for all the encouragement, distraction, love and great times such as outdoors trips and fun days off.

Delft, University of Technology R.M. Storm
April 4, 2018

Table of Contents

List of Figures

List of Tables

Acronyms

ABL	Atmospheric Boundary Layer
ADM	Actuator Disk Model
ADMR	Actuator Disk Model with Rotation
ALM	Actuator Line Model
BEM	Blade Element Model
CFD	Computational Fluid Dynamics
FAST	Fatigue, Aerodynamics, Structures and Turbulence
FLORIS	FLOw Redirection and Induction in Steady state
LCOE	Levelized Cost Of Energy
LES	Large Eddy Simulation
LUT	Look Up Table
NREL	National Renewable Energy Laboratory
NS	Navier-Stokes
OAT	One At a Time
PALM	PArallelized LES Model
RANS	Reynolds-Averaged Navier-Stokes
RMS	Root Mean Sqaure
SLSQP	Sequential Least SQuares Programming
SOWFA	Simulator for Onshore/Offshore Wind Farm Applications
TUD	Delft University of Technology

Chapter 1

Introduction

1-1 Motivation

Every power plant or energy producing facility has an upper limit for energy production, which is called the nameplate capacity. The nameplate capacity is the energy that a power source would produce if it could operate at its maximum energy production all the time without any interuption. However, no power source can actually reach its nameplate capacity. For traditional energy sources, such as hydrocarbons or nuclear, there is maintenance on the equipment, energy demand, and other factors that determine the actual energy that is produced at any given facility. The ratio between the actual energy that is produced and the maximum energy that could be produced in any given time span is called the capacity factor [Beiter et al., 2017].

Renewable energy sources such as wind, solar or hydro have capacity factors that are very sensitive to the availability of their respective power sources. Wind in particular is not only dependent on the strength of the available wind but also on the wind direction. It is usually economically advantageous to group wind turbines together in a wind farm. However, the close proximity of the wind turbines also causes an issue for the capacity factor.

When a wind turbine extracts energy from the atmosphere, a wake forms behind that turbine. The wake is a region with reduced wind velocity and increased turbulence. If a downwind turbine is positioned inside or partially inside a wake, it can usually not operate at its nameplate capacity due to the reduced wind speed. Currently, every turbine tries to maximize its own power production. This is called greedy control, where each turbine aligns with the wind direction and adjusts the blade pitch and generator torque in order to extract as much energy as possible from the wind. A good explanation of this control scheme, which optimizes the power production of a single turbine, can be found in [Johnson, 2004]. This can happen at the expense of the energy production of downwind turbines, which end up in the wake of upwind turbines.

Research has been done towards the reduction of wake-induced energy losses in wind farms [Gebraad et al., 2017]. Previous efforts have focused on redirecting wakes by misaligning an

upwind rotor with the wind direction. This causes the rotor thrust to deflect the wake. The misaligned turbine produces less energy but, if misaligned in such a way that its wake now misses a down wind turbine, the total production of the two turbines increase. Most of these investigations have focused on misaligning the turbine through yaw. This makes sense because the existing commercial turbines readily include yaw motors, in order to align the turbines with the wind.

Harvesting more energy using optimized yaw control compared to greedy control might be possible with existing hardware [Gebraad and Wingerden, 2015] and [Annoni et al., 2016]. The techniques being developed can theoretically be implemented anywhere where wind energy production is deteriorated by wake interactions. This means that farm wide control has potential value and is worth investigating. It is known that in a small scale experimental setup, the total energy production can be optimized by a controller that takes just the first downwind turbine into account [Campagnolo et al., 2016]. In this particular research a line of three turbines produced 15% extra power compared to greedy control.

Since yaw controlled wake redirection can increase the total power production of a wind farm, this additional energy must come from somewhere. Yaw redirection is most effective when the wind direction is aligned with the turbine rows. In this condition high velocity air passes through the empty space between the turbines. Yaw redirection can be thought of as an attempt to redirect those high velocity streams onto downwind rotors. Tilt redirection has the potential to more efficiently use the high velocity air that would otherwise pass over the wind farm. These observations make turbine tilt a worthwhile topic to investigate, especially in the context of optimizing the power production of large wind farms. In a large wind farm the high velocity air between turbines will be used for energy production if the wind farm rows are not completely aligned with the wind direction and the wind farm is large enough. Rotor tilt induced wake redirection might be able to effectively use high velocity air that would otherwise pass unused over a wind farm.

To find optimal turbine control settings in ever-changing wind conditions an optimization algorithm is required. Such an algorithm will likely require a simple and quick wind farm model that models the far wake reasonably accurately. How this process works in detail can be found in [Gebraad et al., 2017]. The algorithm optimizes turbine control settings for the mathematical model. These control settings are then applied to the real wind farm to optimize energy production. Some models include turbine blade loading which can also be taken into account by an optimization routine. Work on these type of controllers is also currently being done at the Delft University of Technology (TUD), for example [van Dijk et al., 2016].

The efficiency of a farm-wide controller is dependent on the models it uses to predict wind farm behaviour. There are several models that can be used for wind farm modeling [Boersma et al., 2016] and [Annoni et al., 2014].

1-2 Objective

This work focuses on the development and implementation of a wake model that can be used to predict the effects of turbine tilting on the wake position. This model can then be used to optimize the control settings of wind turbines in a wind farm, in order to optimize the farm wide energy production. The main objective is to implement the effects of rotor tilt on the

wake and turbine power production in a reduced order model and verify the validity. The objectives of the work presented in this thesis are:

1. Implement the effects of rotor tilting on the wake and turbine power production in a reduced order model
2. Investigate the validity of the model and tune the model to high fidelity simulations
3. Perform a case study in which the total power yield of a small wind farm is optimized using turbine tilt
4. Program the new extension in such a way that the model is modular and easily extendable. Open-source this model such that other people can make use of it.

1-3 Outline

The thesis consists of seven chapters. The first chapter is this introduction. In chapter two the original sub models on which the FLOw Redirection and Induction in Steady state (FLORIS) model is based are explained. Chapter three contains a detailed description of the FLORIS model, both the original implementation as published in [Gebraad et al., 2014] and the recently published analytical wake model as described in [Bastankhah and Porté-Agel, 2016] which is now also part of FLORIS. Chapter four proposes a method of implementing rotor tilt into the FLORIS model. Chapter five contains a sensitivity analysis and an attempt to fit the model. Chapter six details a case study to study the behaviour of the model. Chapter seven contains a conclusion for the thesis.

Chapter 2

FLORIS Origins

The original FLOw Redirection and Induction in Steady state (FLORIS) model, as described in [Gebraad et al., 2014] and [Gebraad et al., 2016], is a wind farm model based on three sub-models. This chapter will describe the models that are the basis for this original implementation. The Gebraad model is an extension of the linear wake model called the Jensen model, as described in [Jensen, 1983]. The Jensen model is based on actuator disk theory which is explained in the first section of this chapter. The Gebraad model computes the speed of overlapping wakes are according to the model in [Katic I., 1986]. Next to these two models is one more sub model to describe the effects of turbine yaw-misallignment. The yaw-misalignment model was first described in [Jiménez et al., 2009] and is called the Jimenez deflection model.

Every section in this chapter describes one of the models. The next chapter will explain how they are merged to form FLORIS. FLORIS was chosen as a starting point for this thesis because it already has a division between these three sub models. This makes it a good fit to extend and implement other velocity and deflection models if that seemed necessary.

2-1 Actuator Disk Model (ADM)

The ADM is one of the most common rotor models. It is widely used because of its simplicity and solid theoretical background. The theory describing the model goes back to 1919 when Albert Betz formulated Betz's law. It was later published in his book [Betz, 1926].

Actuator disk theory is based on the conservation of mass and the assumption of incompressibility of the air flow. A control volume is defined where the pressure drops and the stream velocity is reduced. In the middle of the volume is the actuator disk which extracts momentum from the flow. Figure 2-1 shows a schematic of the ADM. This method abstracts away most details of an actual turbine. The only effect of the turbine in this model is a pressure drop that occurs across the disk. The interactions of the flow with turbine elements such as the tower and nacelle are not modelled at all.

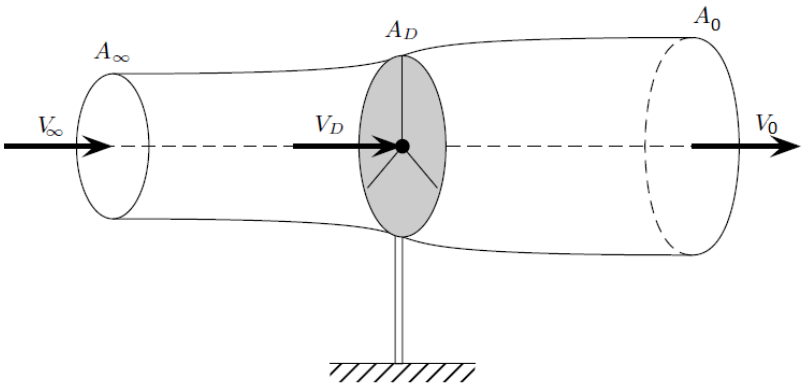

Figure 2-1: Schematic of ADM. Airflow through an actuator disk. [Bianchi et al., 2007]

In Figure 2-1 V_∞ is the inflow speed of the freestream. V_0 is the final flow velocity. V_D is the velocity at the disk. The areas A corresponding to these three velocities are labeled with a matching subscript.

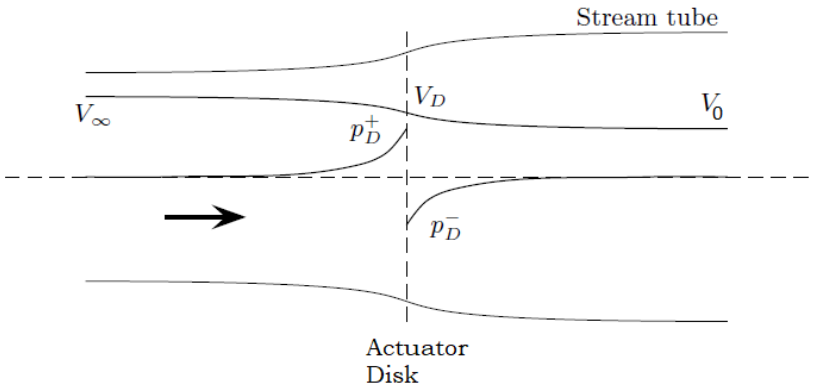

Figure 2-2: Schematic of pressure and velocity drop ADM. [Bianchi et al., 2007]

In Figure 2-2 the velocity and pressure of the stream are plotted. The definitions of the velocities V are identical to those in Figure 2-1, P_D^+ is the pressure before interaction with the actuator disk and P_D^- the pressure after. Eq (2-1) states that the mass flow inside the control volume is conserved. This equation is only valid if the density is constant.

$$\dot{m} = \rho A_\infty V_\infty = \rho A_D V_D = \rho A_0 V_0 \tag{2-1}$$

The turbine is the only element in the control volume that exerts force on the flow. This force can be computed by multiplying the mass flow with the velocity difference as shown in (2-2). Another method of computing the force is multiplying the pressure drop with the rotor area.

$$F_D = \rho A_D V_D (V_\infty - V_0) = (p_D^+ - p_D^-) A_D \tag{2-2}$$

The previous equations do not give an easy method to compute the velocity drop or the turbine force. Turbine control usually relies on two non dimensional coefficients called the

thrust and power coefficient. The thrust coefficient is the ratio of the turbine thrust with the airflow thrust. The power coefficient is the ratio between power extracted by the turbine and the total power in the flow. These coefficients are important indicators of how the turbine is behaving. The power coefficient reflects how much of the available energy is extracted from the airflow. The thrust coefficient represent how much the flow is affected by turbine operation. Both coefficients are abstractions of actual turbine characteristics such as generator torque and the pitch angle of the blades.

The definition of the thrust coefficient is shown in (2-3) and of the pwoer coefficient is shown in (2-4).

$$C_T = \frac{\rho A_D V_D (V_\infty - V_0)}{\frac{1}{2}\rho A_D V_\infty^2} \tag{2-3}$$

$$C_P = \frac{\frac{1}{2}\rho A_D V_D (V_\infty^2 - V_0^2)}{\frac{1}{2}\rho A_D V_\infty^3} \tag{2-4}$$

These expressions can be simplified but even then, calculations will stay involved. Axial interference is a factor relating the different windspeeds in the model to eachother. This simplifies the calculations. This factor is also called the axial induction factor or the axial flow interference factor or simply a. It is defined as shown in (2-5).

$$V_D = (1 - a)V_\infty \tag{2-5}$$

Note that the axial interference factor is not a directly measurable parameter. It is an abstraction of the turbine function which is useful to describe and control turbine behaviour.

After some derivations that will be omitted here the final velocity and the power and thrust coefficients can be computed quite concisely as shown below. To see the full derivations please see [Bianchi et al., 2007].

$$V_0 = (1 - 2a)V_\infty \tag{2-6}$$

$$C_T = 4a(1 - a) \tag{2-7}$$

$$C_P = 4a(1 - a)^2 \tag{2-8}$$

The model has some obvious shortcomings. Real turbines are not confined in a streamtube and they have individual blades that cause turbulence. Furthermore any condition except for a uniform inflow orthogonal to the turbine cannot be modeled. The model is however simple to understand and has a very strong theoretical basis. It can be used to compute the theoretical maximum power coefficient. This is called the Betz limit and occurs at $a = \frac{1}{3}$ with $C_P = \frac{16}{27} = 59.3\%$. It can be implemented in high fidelity CFD simulators and is used as the basis for several parametric models.

2-2 Jensen model

The Jensen model is one of the first steady state flow models. It was first published in 1983 [Jensen, 1983] and has been in use since than. Figure 2-3 shows a schematic representation of the Jensen model. It is based on conservation of momentum as described in (2-9). V_0 is the reduced flow velocity immediately behind the turbine. The Jensen model takes the final velocity as predicted by actuator disk theory and assumes that the wake starts with that velocity. V_∞ is the velocity of the surrounding flowfield and r_0 is the initial wake radius. V_w is the wake velocity at the place where the wake diameter is r. A linear relationship between distance from turbine x_d and wake diameter r is assumed in this model.

$$\pi r_0^2 V_0 + \pi(r^2 - r_0^2)V_\infty = \pi r^2 V_w \tag{2-9}$$

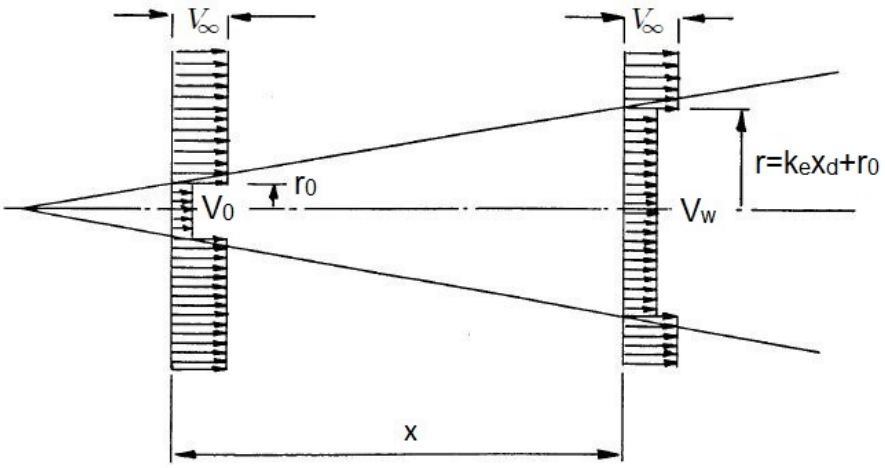

Figure 2-3: Schematic representation of Jensen wake model, symbols are explained in text. Figure taken from [Jensen, 1983]

The Jensen model needs just two parameters. The first one is the axial induction that determines the ratio between V_0 and V_∞ as shown in (2-6), it is repeated here for clarity. This equation comes from standard actuator disk theory as described in [Bianchi et al., 2007] and Section 2-1. In [Jensen, 1983] an optimal $a = 1/3$ is assumed, but a can also vary per turbine. The difference between the ADM and Jensen is that the pressure drop in Jensen is instantaneous. The axial induction a can be computed based on the power production of a turbine by using (2-4). This first parameter in Jensen is therefore not a fitting parameter. In some turbine types it can be actively controlled by adjusting the power production of the turbine and in other turbines it is simply a function of the turbine operation and inflow conditions.

$$V_0 = (1 - 2a)V_\infty \tag{2-6}$$

The second parameter in the Jensen model is the wake expansion coefficient k_e that determines the radius $r(x_d)$ of the wake. This parameter has to be fitted on data. Either by gathering measurements from a windfarm or by simulating a windfarm in a Computational

Fluid Dynamics (CFD) model to generate flowdata. Equation (2-9) can be rewritten to solve explicity for the velocity V_w at some point x_d inside the wake. This is shown in (2-10).

$$V_w(x) = V_\infty \left(1 - 2a\frac{r_0^2}{(k_e x_d + t_0)^2}\right) \tag{2-10}$$

The model is simple but also limited. In reality, the near wake is not a steady and slow velocity field. That region is dominated by turbulent effects and asymmetries caused by the turbine blades in addition to a pressure drop and slowdown of the air. Jensen is not usable to describe that region. Furthermore, the speed profile is described as a perfect cone which leaves a cut-through of the velocity profile looking like a top-hat. This makes for easy computation but is not realistic enough in most situations. In the original paper [Jensen, 1983] a method is proposed to remove the discrete boundaries of the wake by using a cosine bell function to change the velocity profile.

In [Jensen, 1983] two situations with wake overlap are demonstrated. Full wake overlap is assumed and the input speed for a downstream rotor is simply taken as the wake speed of the upwind turbine. Multiple fully overlapping wakes are also demonstrated. This calculation becomes really involved with even a few wakes. Therefore, the original model assumes full wake recovery in a rather short distance to keep the computations tractable. This means that if a wake is approximately ten rotor diameters behind the turbine, it's influence is neglected in [Jensen, 1983]. These wake interaction calculations cannot take partial wake overlap into account.

2-3 Wake Interaction

Katič co-wrote a paper with Jensen describing the efficiency of a cluster of wind turbines [Katic I., 1986]. A method for combining wakes is proposed in that paper. The windspeed inside a wake according to Jensen is only dependent on it's downwind distance from the turbine. It can be equivalently described as a stream with an energy deficit with respect to the free stream V_∞. If two wakes overlap at any point, their energy deficits can be summed to compute the total energy deficit at that point as shown in (2-11). V_p^1 and V_p^2 are the speeds predicted for two wakes at some point p. V_p is the combined predicted speed at that point. Note that V_p/V_∞ is the relative velocity, $1 - V_p/V_\infty$ is the relative velocity deficit and $(1 - V_p/V_\infty)^2$ is called the relative kinetic energy deficit.

$$(1 - V_p/V_\infty)^2 = (1 - V_p^1/V_\infty)^2 + (1 - V_p^2/V_\infty)^2 \tag{2-11}$$

If multiple wakes overlap at any point all the energy deficits can simply be added to compute some resultant velocity at that point. Rewriting (2-11) to solve for the combined velocity V yields (2-12). Equation (2-12) also sums the relative kinetic energy deficits over the wake prediction of k turbines instead of just two predictions as shown in (2-11).

$$V_p = V_\infty \left(1 - \sqrt{\sum_k (1 - V_p^k/V_\infty)^2}\right) \tag{2-12}$$

In [Katic I., 1986] the method is shown to be valid on a cluster of 630 kW turbines. This computation does however raise a problem. Adding deficits makes it possible for the stream to have negative energy and thus imaginary velocity. This cannot happen in reality.

It also seems counter intuitive that V_p is not only dependent on V_p^1 and V_p^2 but also on V_∞. A higher V_∞ for equal V_p^1 and V_p^2 implies a greater energy deficit and thus a lower estimated combined velocity. Figure 2-4 shows how the model expects the velocity to change dependent on a changing V_∞.

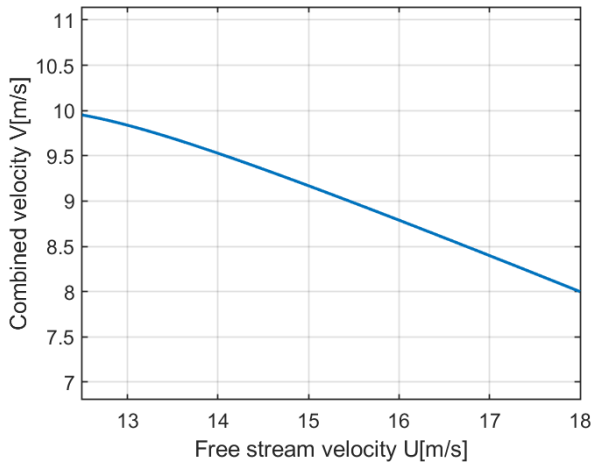

Figure 2-4: Calculated velocity of combined wake through energy deficits, $V_p^1 = 10$ m/s, $V_p^2 = 12$ m/s

Doing wind tunnel experiments, field tests or running simulations with more accurate models such as Large Eddy Simulation (LES) programs can help to understand the validity and limits of adding energy deficits. At least one such study has been done [Machefaux et al., 2015]. Their main conclusion is that the accuracy of the wake summation approach is dependent on the inflow velocity. At low velocities the wake deficits are relatively large and linear summation of the velocity deficits works well. At higher velocities wake deficits are less pronounced and quadratic summation of wake deficits is more accurate. However this reasoning is dependent on their turbine choice which is a stall regulated turbine with constant rotational speed and pitch. It is difficult to generalize from their results and define a better method for wake combination. Future research could yield improvements in this area.

2-4 Wake deflection through yaw misalignment

[Jiménez et al., 2009] describes a method for extending the principles behind the Jensen model to calculate the effects of yaw misalignment on wake position. An initial wake angle θ_{init} is computed based on the thrust coefficient C_T and yaw angle γ as shown in (2-13). This equation is derived by estimating the forces on a redirected wake and equating them to the rotor forces at the turbine. A schematic of these forces is shown in Figure 2-5.

$$\theta_{\text{init}}(a, \gamma) = \frac{1}{2} \cos^2(\gamma) \sin(\gamma) C_T(a) \tag{2-13}$$

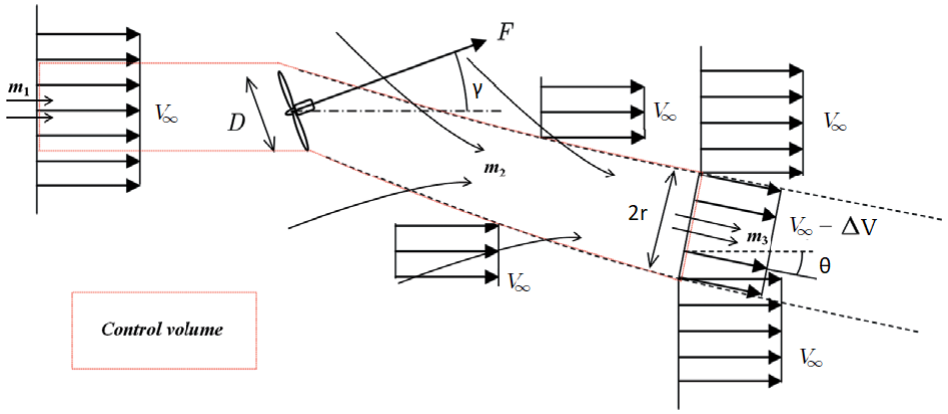

Figure 2-5: Simplified representation of the momentum conversation-based model for the wake angle. source [Jiménez et al., 2009]

An equation describing the angle of the wake at downwind distance x_d from the turbine is also derived and shown in (2-14). The term $r(x_d) = 2k_e x_d + r_0$ is identical to the wake radius in the Jensen model. This computation relies on the same assumptions as the Jensen model. As explained before, it is only useful for describing far wake behaviour.

$$\theta(x_d) = \frac{\theta_{\text{init}}}{\left(\frac{2r(x_d)}{D}\right)^2} \tag{2-14}$$

The wake angle estimation is dependent on other assumptions in addition to the Jensen model assumptions. Specifically to compute the forces that deflect the wake [Jiménez et al., 2009] makes two assumptions are at least partially invalid.

1. The sine of the wake angle is approximately equal to the wake angle $sin(\theta) \approx \theta$
2. The wake velocity deficit is very small compared to the free stream, $\Delta V << V_\infty$

The wake velocity deficit is computed using Jensen and is dependent on the downstream distance. The region where the deflected wake is being deflected back along the stream wise direction has velocity deficits that are large in comparison to the free stream.

Another issue with the model is a basic assumption of the Jensen model. At inlet and lateral boundaries, an unperturbed field of wind velocity, of magnitude V_∞ and parallel to free stream is assumed. Since the wake is deflected the inflow can probably not be modeled as being along the free stream direction.

Chapter 3

FLORIS

This chapter consists of two sections. The first section covers the original implementation of the FLOw Redirection and Induction in Steady state (FLORIS) model as described in [Gebraad et al., 2014]. The second section will be a concise explanation of the analytical wake model as described in [Bastankhah and Porté-Agel, 2016]. The third section will described some additional options that can be used to model the velocity profile for a wake and some other options for summing wakes.

3-1 Originial FLORIS Model

The model in this section is based on the three models described in Chapter 2. These sub-models form a nice conceptual division for any wind farm model. The first subsection here will explain how the wake velocity profile is described. The second subsection will explain how the wake deflection model is practically implemented. The third subsection described how the wakes are summed to compute the averaged inflow velocity on any downwind rotor.

3-1-1 Wake Velocity Profile

The wake model described in Section 2-2 has a discrete border between the wake and the free stream. furthermore, the velocity inside the wake is only dependent on the downwind distance. In reality, the velocity in a wake is faster near the edge and the transition to the free stream is smooth. To improve on the Jensen model, FLORIS makes use of three zones. The wake is still axisymmetric in this model but when moving from the center line of the wake to the edge there are two additional discrete boundaries. This is shown in Figure 3-1.

The original paper of the Jensen model [Jensen, 1983] proposes to change the tophat velocity profile with a continuous curve. But this is difficult to implement since a 2D gaussian curve has no analytical solution to the volume of a circular region. Splitting the wake into three distinct wake zones as show in Figure 3-1-b is a much better fit than a tophat [Gebraad et al., 2016]

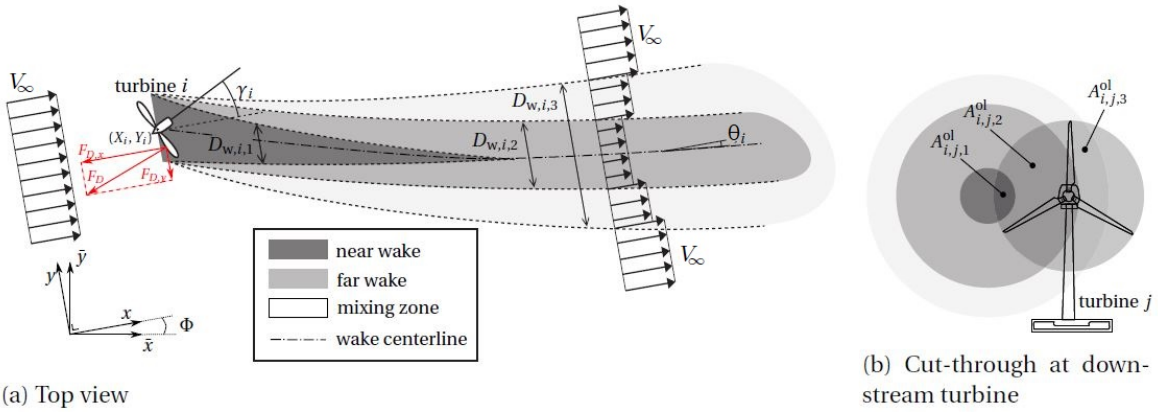

(a) Top view

(b) Cut-through at downstream turbine

Figure 3-1: Schematic of FLORIS. Shown are the different wake zones, yaw effects and wake overlap on downstream turbine. source[Gebraad et al., 2016]

and does have an analytical solution. However, the additional zones also introduce additional fitting parameters.

In the Jensen model the expansion parameter also governs the rate of wake recovery. The multi-zone wake velocity model breaks this straightforward relationship. Every zone of the wake now requires a parameter to described how quickly that part of the wake recovers velocity. The recovery coefficients are fitted in such a way that the velocity increases with each zone that is closer to the boundary of the wake. The wake recovery coefficient of the inner zone, also called the near wake, thus has the lowest recovery coefficient.

The multi-zone implementation takes a base expansion coefficient k_e and has a multiplier $m_{e,q}$ per zone where the subscript q is the zone number. The diameter of a wake zone at some location x_d is defined as shown in (3-1). The constants D and X_i are the initial wake diameter and the X-coordinate of turbine i respectively. The initial wake diameter is taken to be equal to the turbine blade diameter. Since the FLORIS model usually has multiple turbines the downwind distance x_d is replaced with the term $x_d = x - X_i$ where x now denotes an arbitrary reference frame. When computing the wake diameter or velocity the sub-models require the downwind distance with respect to a turbine i.

$$D_{w,i,q}(x) = \max(D + 2k_e m_{e,q}(x - X_i), 0) \tag{3-1}$$

The general form for the wake velocity V_w^i at some point (x_d, r) according to turbine i is shown in (3-2). V^i is the computed inflow speed of the turbine. a_i is the axial induction factor of this turbine as described in section 2-1. c_i is a recovery coefficient dependent on turbine i, downwind distance x_d and radial distance from the wake centerline r.

$$V_w^i(x_d, r) = V^i(1 - 2a_i c_i(x_d, r)) \tag{3-2}$$

Notice that (3-2) is very similar to (2-10). The only difference is that the inverse square relationship between downwind distance x_d and wake velocity V_w is more complicated here

due to the multiple zones. The wakezones are all defined by their diameter (3-1) and the wake recovery coefficient is unique per turbine per zone and is computed as shown in (3-3) and (3-4).

$$c_i(x_d, r) = \begin{cases} c_{i,1} & \text{if} \quad r \leq D_{w,i,1}/2 \\ c_{i,2} & \text{if} \quad D_{w,i,1}/2 < r \leq D_{w,i,2}/2 \\ c_{i,3} & \text{if} \quad D_{w,i,2}/2 < r \leq D_{w,i,3}/2 \\ 0 & \text{if} \quad r > D_{w,i,3}/2 \end{cases} \tag{3-3}$$

$$c_{i,q}(x_d) = \left(\frac{D_i}{D_i + 2k_e m_{U,q}(\gamma_i) x_d} \right)^2 \tag{3-4}$$

In (3-4), $m_{U,q}(\gamma_i)$ is a yaw dependent decay coefficient defined in (3-5). The coefficients $m_{U,q}$ are three fitting parameter that describe how quickly each wake zone q decays with increasing downwind distance x_d. In [Gebraad et al., 2016] these three parameters are estimated to be [.5 1 and 5.5] respectively. These values are manually tuned to fit the multi-zone wake model on Simulator for Onshore/Offshore Wind Farm Applications (SOWFA) data while siulating an NREL 5MW turbine.

$$m_{U,q}(\gamma_i) = \frac{M_{U,q}}{\cos(a_U + b_U \gamma_i)} \tag{3-5}$$

The previous equations describe the recovery of the wake deficit for each wake zone. However V^i is only defined for the turbines that have an undisturbed inflow. For those turbines V^i is simply the free stream velocity V_∞. If a turbine is positioned downwind of other turbines its inflow velocity V^i needs to be computed by taking those upstream wakes into account. How this procedure works is explained in Section 3-1-3.

3-1-2 Wake Centerline Position

In Section 2-4 a formula for the wake angle θ is presented. Integrating the tangent of this angle gives the yaw induced centerline displacement in the y-direction. See (3-6).

$$\delta y_{w,yaw,i}(x) = \int_0^{x - X_i} \tan(\theta_i(x)) dx \tag{3-6}$$

There is no analytical solution to this expression. For this reason, the second order Taylor series expansion of the tangent is used. The result is shown in (3-7).

$$\delta y_{w,yaw,i}(x) \approx \frac{\theta_{init}(a_i, \gamma_i) \left(15 \left(\frac{2k_e(x - X_i)}{D_i} + 1 \right)^4 + \theta_{init}(a_i, \gamma_i)^2 \right)}{\frac{30k_e}{D_i} \left(\frac{2k_e(x - X_i)}{D_i} + 1 \right)^5} - \frac{\theta_{init}(a_i, \gamma_i) D_i \left(15 + \theta_{init}(a_i, \gamma_i)^2 \right)}{30k_e} \tag{3-7}$$

The yaw misallignment of the turbine is not the only factor contributing to the wake centerline displacement. The rotation of the turbine blades exert an asymmetrical force on the airstream which is modeled as a linear displacement as shown in (3-8).

$$\delta y_{w,rotation,i}(x) = a_Y + b_Y(x - X_i) \tag{3-8}$$

Modeling $\delta y_{w,rotation,i}$ using a linear function means that the wake angle never reaches 0 with respect to the flowfield. When $x - X_i \to \infty$ the wake angle $\theta \to \tan^{-1}(b_d)$, since the wake will eventually fully recover this is not correct. However $b_d \approx .01$ is small and the wake velocity recovers such that the wake displacement becomes irrelevant at some point since the wake disappears $V_w \to V_\infty$. The current expression also adds two parameters to FLORIS which means fitting the model becomes more challenging. A paper trying to optimize FLORIS for gradient based optimization replaced this expression with one that does decay to zero [Thomas et al., 2016]. Improving the estimation of the rotation induced deflection is probably possible but what sort of approach is most promising is not clear.

Adding (3-7) and (3-8) gives the total wake centerline deviation with respect to the turbine hub as estimated by FLORIS. Adding the position of the turbine Y_i gives the y-coordinate of the wake centerline for an x-coordinate as shown in (3-9).

$$y_{w,i}(x) = Y_i + \delta y_{w,yaw,i}(x) + \delta y_{w,rotation,i}(x) \tag{3-9}$$

3-1-3 Wake summation

With the wake velocity prodile and wake centerline position defined there is one last part of the FLORIS model that needs explaining. As explained at the end of Section 3-1-1, when turbine i is positioned downstream from other turbines its inflow velocity V^i needs to be computed based on those upstream turbines. FLORIS handles this problem by checking which wakes and wakezones cover parts of the rotor swept area. These are than combined as described in [Katic I., 1986]. For clarity the main result of the [Katic I., 1986] paper, equation (2-12), is repeated here.

$$V_p = V_\infty \left(1 - \sqrt{\sum_k (1 - V_p^k/V_\infty)^2}\right) \tag{2-12}$$

Equation (2-12) is not directly implementable in FLORIS. The terms V_p^k refer to the velocity at some point p but for FLORIS the velocity on the entire swept area of a rotor needs to be known. Furthermore in (2-12) every velocity prediction V_p^k is normalized with respect to the free stream velocity V_∞. However, (3-2) shows that a wake as predicted by FLORIS can never reach a higher velocity than its inflow velocity V^i. Therefore, its wake deficit should also be normalized with respect to its inflow velocity, otherwise a constant velocity deficit will remain while the wake has fully recovered. Equation (3-10) shows a general form for the inflow velocity V^i for any turbine i. The symbols $\mathcal{F}$, $\mathcal{U}$ and $\mathcal{D}$ denote turbine sets with all the turbines, upwind turbines and downwind turbines respectively. If a turbine i is positioned

such that there are turbines upstream, $X_n < X_i$, their velocity predictions at turbine i are summed.

$$V^i = \begin{cases} V_\infty & \forall i \in \mathcal{U} \\ V_\infty - \sqrt{\sum_{n \in \mathcal{F}: X_n < X_i} \left(1 - V_i^n / V^n\right)^2} & \forall i \in \mathcal{D} \end{cases} \tag{3-10}$$

Equation (3-11) show how (3-2) is changed such that the size of the wake overlap with the rotor is taken into account. The term $A_{n,i,q}^{ol}$ is the area of a wake zone caused by turbine n that covers a part of the swept area of turbine i as shown in Figure 3-1.

$$V_i^n = V^n \left(1 - 2a_i \frac{\sum_{q=1}^{3} c_{i,q}(x_i - x_n) A_{n,i,q}^{ol}}{A_i}\right) \tag{3-11}$$

This concludes the originial implementation of the FLORIS model. The wake veloicty model described in Section 3-1-1 will be called the multi-zone wake model from here on. The deflection model as described in Section 3-1-2 is called the Jimenéz model.

3-2 self similar wake model

A new wind farm model based on the conservation of mass and momentum has been proposed in [Bastankhah and Porté-Agel, 2014]. This work has later been extended by Amin Niayifar and Porté-Agel in [Niayifar and Porté-Agel, 2015]. This second version implemented a model to calculate the local turbulence intensity in the wind farm instead of using the turbulence intensity as a fitting parameter for the whole wind farm. In addition the wake combination procedure was changed from summing energy deficits to the velocity deficit superposition principle. Most recently, this model has been analyzed and extended by studying the budget of the Reynolds-Averaged Navier-Stokes (RANS) equations and measuring the wake characteristics of a scaled down wind turbine in [Bastankhah and Porté-Agel, 2016]. The budget analysis provides insight into how the terms in the RANS equation balance out when there is a yaw induced lateral flow.

The latest version, described in [Bastankhah and Porté-Agel, 2016], is implemented in FLORIS as well. The velocity profile is called the Gaussian wake from here on out. The deflection model will be called the Bastankhah and Porté-Agel deflection model. This model shows good agreement with Large Eddy Simulation (LES) simulations of the wake deflection and the rate of wake recovery. According to the LES data gathered in [Bastankhah and Porté-Agel, 2016], the Jiménez wake deflection model proposed in [Jiménez et al., 2009], often overestimates the amount of deflection caused. The new deflection model does not seem to suffer from this problem. The self similar solution to the Navier-Stokes (NS) equations that describes the steady state flow behind an actuator disk as a Gaussian. A Gaussian shows better agreement with experimentally measured wakes than the discrete zones originally used in FLORIS. Other advantages include, fewer tuning parameters and a continuous solution which can help during optimization.

Figure 3-2 is a schematic representation of the Porté-Agel model. The model consists of a near wake and a far wake. The near wake is modelled as a constant velocity core that

dissipates into a Gaussian velocity profile around it. This idea comes from the study of jet flows [Rajaratnam, 1977]. The far wake expands linearly with downwind distance, it's wind speed deficit decays quadratically. Figure 3-3 shows the predicted wake for a turbine with 25° yaw. The near-wake standard deviation in the y-direction, σ_{y_0}, scales with the cosine of the yaw angle while σ_{z_0} remains constant. This means that the wake will become an axisymmetrical ellipse under yawed conditions. It is not very visible in Figure 3-3 because even at 25° $\sigma_{y_0} = \cos(25°) \cdot \sigma_{z_0} = 0.9 \cdot \sigma_{z_0}$, the width of the wake is still 90% of the height of the wake.

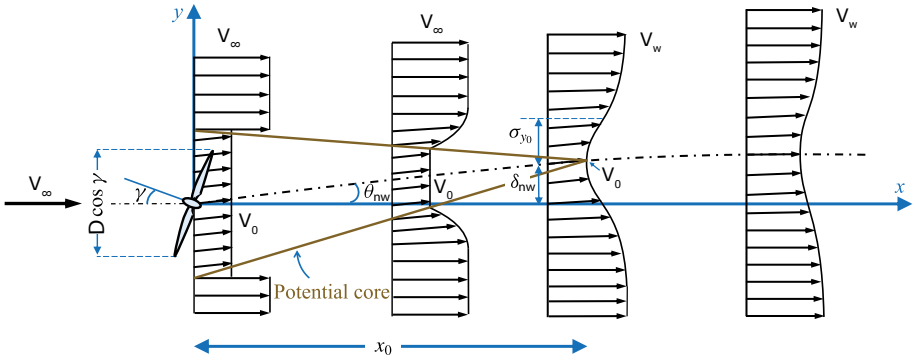

Figure 3-2: Schematic cut-through of Porté-Agel model at hub-height, [Bastankhah and Porté-Agel, 2016]

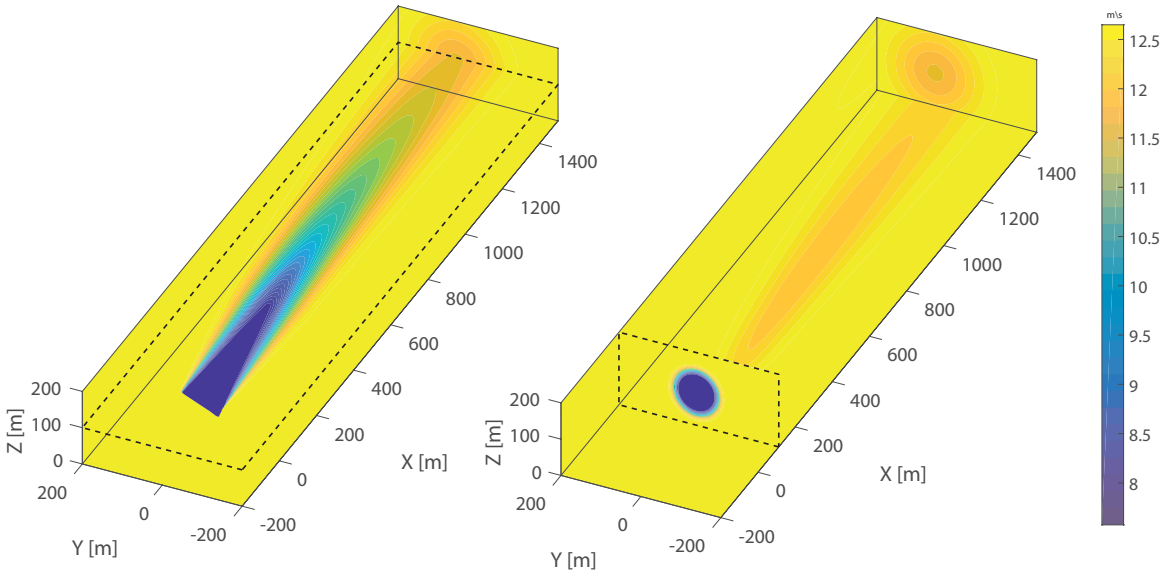

Figure 3-3: x-y cut-through of wake on hub-level and y-z cut-through at 100m behind turbine

The model will be described over the course of the next four subsections. The four topics are listed below.

- Where is x_0, the transition point between the near wake and far wake?
- How is the velocity profile in the near wake defined?

- What are the intensity and standard deviation of the far-wake?
- How do the near and far wake deflect?

Each subsection will answer one of these questions.

3-2-1 Transition between near wake and far wake

The streamwise distance that defines the end of the near-wake core, x_0, is defined in (3-12). It is based on a generalization of a formula describing the width of the shear layer around a core found by [Lee & Chu, 2003] in the context of turbulent jets.

$$x_0 = \frac{\sqrt{2} \cdot R \cdot \cos(\gamma)(1 + \sqrt{1 - C_T})}{\alpha \cdot I + \beta(1 - \sqrt{1 - C_T})} \tag{3-12}$$

Where α and β are fitting parameters that can adjust the near-wake length. Jet flow studies find a value of $\beta = 0.154$. [Bastankhah and Porté-Agel, 2016] found a value of $\alpha = 2.32$ to fit the near-wake core length on experimental turbine data. These parameters are probably not fully generalized and thus may require adjusting for different turbines or atmospheric conditions.

Furthermore x_0 is dependent on the incoming streamwise turbulence intensity I at hub height. This parameter varies from 0 to 1, respectively, ideal laminar conditions and an exclusively turbulent flow. [Niayifar and Porté-Agel, 2015] describes various parametric models that estimate this value. The models described there all predict an added turbulence intensity from every upwind rotor. The total incoming streamwise turbulence intensity I is found by taking the norm of the ambient turbulence and all the added turbulence intensities as shown in (3-15). The added turbulence from rotor k is shown in (3-14) this formula come from [Crespo and Hernández, 1996]. According to [Niayifar and Porté-Agel, 2015] using this expression is the most accurate when compared to LES data. The added turbulence intensity of turbine k is normalized with the relative overlap $\frac{A_k}{A}$ of the wake and the swept area of the turbine in question. If there are no upwind turbines or none of the wakes of upwind turbines overlap this turbine, I reduces to I_0.

$$I_k^+ = I_a a^{I_b} I_0^{I_c} \left(x_d/D\right)^{I_d} \tag{3-13}$$

$$I_k^+ = .73 a^{.8325} I_0^{.0325} \left(x/D\right)^{-.32} \tag{3-14}$$

$$I = ||\frac{A_1}{A} I_1^+, \cdots, \frac{A_n}{A} I_n^+, I_0|| \tag{3-15}$$

3-2-2 Near-Wake Velocity Profile

The velocity in the core of the near wake is dependent on the thrust coefficient C_T as shown in (3-16). It is currently unclear if C_T should be adjusted for the turbine yaw in this equation. The normalized velocity deficit, C_0, corresponding to the wake velocity V_0 is also shown in (3-16).

$$
\begin{aligned}
V_0 &= V_\infty \sqrt{1 - C_T} \\
C_0 &= 1 - \frac{V_0}{V_\infty} = 1 - \sqrt{1 - C_T}
\end{aligned}
\tag{3-16}
$$

The normalized velocity deficit C_0 is a useful measure because the deficit decays in the y- and z- direction when you move further away from the near-wake core. As the core radius itself decays along the x-direction, the Gaussian that develops around it approaches the Gaussian at the onset of the far wake. The expression for the Gaussian at the end of the near wake is shown in (3-17). In all equations, x_d is the streamwise direction centered at the turbine and positive in the downwind direction. y, the spanwise direction, and z, the vertical direction, are relative to the wake centerline at the current x-coordinate.

$$
\begin{aligned}
\sigma_{z_0} &= \frac{R}{\sqrt{2}} \\
\sigma_{y_0} &= \frac{R}{\sqrt{2}} \cos(\gamma) \\
V_w\big|_{x_d = x_0} &= V_0 \cdot e^{-0.5\left(\frac{y}{\sigma_{y_0}}\right)^2} e^{-0.5\left(\frac{z}{\sigma_{z_0}}\right)^2}
\end{aligned}
\tag{3-17}
$$

The equation for the near-wake velocity profile given in [Bastankhah and Porté-Agel, 2016] is shown in (3-18). r_{pc} denotes the radius of the potential core, since the near-wake core is elliptical it varies with x, y and z. r is the hypotenuse of any (y, z) coordinate with respect to the near-wake centerline $r = \sqrt{y^2 + z^2}$. Beware that in this equation there is some notational handwaving. When a point (y, z) lies outside the potential core its distance $(\Delta y, \Delta z)$ has to be computed. These than have to be divided by σ_{nw}, for the relative y distance from the near-wake core this is $\sigma_{y_0} \frac{x_d}{x_0}$ for the z difference it is $\sigma_{z_0} \frac{x_d}{x_0}$

$$
\frac{V_w}{V_\infty} = \begin{cases} 1 - C_0 & \text{if } r \leq r_{pc} \\ 1 - C_0 e^{-\left(\frac{r - r_{pc}}{2\sigma_{nw}}\right)^2} & \text{if } r > r_{pc} \end{cases}
\tag{3-18}
$$

When implementing these equations, the $r - r_{pc}$ term generates a Gaussian with standard deviation δ_{nw} that starts at the boundary of the ellipse describing the near-wake core. The standard deviation of the near wake, σ_{nw}, increases linearly from 0 at $x_d = 0$ to $\sigma_0 at x_d = x_0$ over the length of the near-wake.

To illustrate this, Figure 3-4 shows the x-y plane of two Gaussians with standard deviation σ_{nw} increasing linearly from 0 to σ_0. The right image lacks a core corresponding to $r_{pc} = 0$ in (3-18). The left image does have a core where r_{pc} denotes the boundary of this core. In the x-y plane shown in Figure 3-4 $r_{pc} = R\cos(\gamma)\,(1 - x/x_0)$, in the x-z plane $r_{pc} = R\,(1 - x/x_0)$. Notice that, because the core radius decays to zero both images end up with the exact same Gaussian distribution at the end of the near-wake, $x_0 \approx 480$[m].

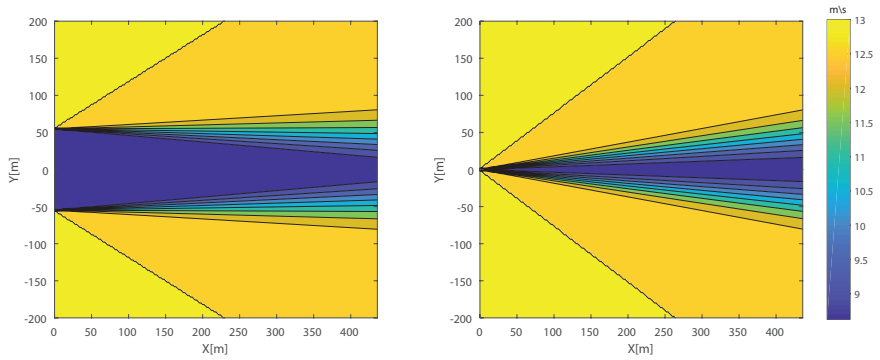

Figure 3-4: Near-wake with (left) and without (right) near-wak core

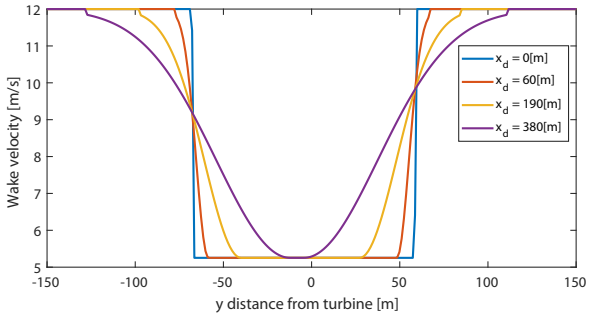

Figure 3-5: Transition from tophat velocity profile to Gaussian

3-2-3 Far-Wake Velocity Profile

The far wake progresses from the Gaussian at $x_d = x_0$, (3-17), into a wider Gaussian whose intensity decays as shown in Figure 3-2 and equation (3-23). The standard deviation of the wake increases linearly in both the y- and z- direction starting from x_0, as shown in (3-21) and (3-22).

$$k_* = k_z = k_y = k_a I + k_b \tag{3-19}$$

$$k_* = 0.3837I + 0.003678 \tag{3-20}$$

$$\sigma_z = \frac{R}{\sqrt{2}} + (x - x_0) \cdot k_z = \sigma_{z_0} + (x - x_0) \cdot k_z \tag{3-21}$$

$$\sigma_y = \frac{R}{\sqrt{2}} \cos(\gamma) + (x - x_0) \cdot k_y = \sigma_{y_0} + (x - x_0) \cdot k_y \tag{3-22}$$

$$\frac{V_w}{V_\infty} = 1 - \left(1 - \sqrt{1 - C_T \frac{\sigma_{z_0}\sigma_{y_0}}{\sigma_z \sigma_y}}\right) e^{-0.5\left(\frac{y(x)}{\sigma_y}\right)^2} e^{-0.5\left(\frac{z(x)}{\sigma_z}\right)^2} \tag{3-23}$$

The term $\frac{\sigma_{z_0}\sigma_{y_0}}{\sigma_z \sigma_y}$ is the ratio between the standard deviations in the y and z direction at the transition point x_0, and at some further downwind position $x_d > x_0$. Since the standard deviations grow with distance this term quadratically approaches zero. This makes the wake recover to the free-stream velocity V_∞. k_y and k_z are both linear functions in I as shown in

(3-20)[Niayifar and Porté-Agel, 2015]. Both the onset of the far wake and the growth rate of the far wake thus depend directly on the turbulence intensity, I. Currently, k_y and k_z are assumed equal because there is not a lot of data about the differences in wake growth in the y- and z-direction, and k_a and k_b are fitting parameters.

3-2-4 Bastankhah And Porté-Agel Wake Deflection Model

The angle of the near wake θ_{nw} is a constant computed using the yaw angle γ and the thrust coefficient C_T. Because θ_{nw} is constant, the near-wake centerline deflection can be modeled as a triangle. Equation (3-24) shows both the near-wake deflection, δ_{nw}, and the near-wake angle, θ_{nw}, upon which δ_{nw} depends.

$$\begin{aligned} \theta_{nw} &= \frac{0.3\gamma}{\cos(\gamma)}\left(1-\sqrt{1-C_T\cos(\gamma)}\right) \\ \delta_{nw}(x) &= x\tan(\theta_{nw}) \approx x\cdot\theta_{nw} \end{aligned} \tag{3-24}$$

The deflection of the far-wake δ_{fw} is a shown in (3-25). This expression is derived by integrating an expression that describes the wake angle based on a result from the RANS equation.

$$\begin{aligned} \delta_{fw} =& \tan(\theta_{c_0})x_0 + R\frac{\theta_{c_0}}{7.35}\sqrt{\frac{\cos(\gamma)}{k_y k_z C_T}}\left(2.9+1.3\sqrt{1-C_T}-C_T\right) \\ &\times \ln\left[\frac{\left(1.6+\sqrt{C_T}\right)\left(1.6\sqrt{\frac{\sigma_z\sigma_y}{\sigma_{z_0}\sigma_{y_0}}}-\sqrt{C_T}\right)}{\left(1.6-\sqrt{C_T}\right)\left(1.6\sqrt{\frac{\sigma_z\sigma_y}{\sigma_{z_0}\sigma_{y_0}}}+\sqrt{C_T}\right)}\right] \end{aligned} \tag{3-25}$$

For more background information and the full derivation of the equations in this section [Bastankhah and Porté-Agel, 2016] should be consulted. However the equations presented in this section are sufficient to implement the model.

In the paper, [Bastankhah and Porté-Agel, 2016], the effects of blade rotation on the wake are discussed initially but are eventually omitted for simplicity. This leads to the wake deflection being zero when the turbine is unyawed. Earlier studies show the unyawed case should have a deflection [Fleming et al., 2014] and [Fleming et al., 2015]. This blade-rotation-induced wake deflection can be fitted using a linear function [Gebraad et al., 2014]. Thus, the Porté-Agel model used in FLORIS has been extended with a linear function fitted to model the blade rotation induced deflection. This means extending (3-24) and (3-25) in the same way as (3-9). Thus, the total deflection as predicted by the Bastankhah And Porté-Agel Wake Deflection Model is shown in (3-26).

$$\delta_{\text{total}} = \begin{cases} \delta_{nw} + \delta y_{w,rotation,i}(x) & \text{if } x \le x_0 \\ \delta_{fw} + \delta y_{w,rotation,i}(x) & \text{if } x > x_0 \end{cases} \tag{3-26}$$

3-3 final remarks

The FLORIS model is now capable of using the multi-zone wake velocity model, the Gaussian wake velocity model and the Jensen velocity model. It can also be used with the Jimenez deflection model or the Bastankhah and Porté-Agel deflection model.

The FLORIS model as available online has some additional options which are not elaborated on in this thesis. There are two additional wake velocity models namely the Larsen model as described in [Larsen, 1988] is also available. Furthermore, a version of the Jensen model where the tophat as been replaced with a Gaussian of equal velocity deficit is also available. In addition to those two wake velocity models several methods of wake addition are available. It would be very interesting to see how these models stack up to each other and in different situations. However, the main topic of this thesis is the implementation of rotor tilting.

The self similar wake model described in the last section consisting of the Gaussian wake velocity model and the Bastankhah and Porté-Agel wake deflection model is better than the original implementation of FLORIS described in Section 3-1. Especially the lower amount of fitting parameters and the fact that these parameters are based on other studies instead of being tuned manually was very promising. Additionally the assumptions underlying the deflection model seem to be better than those of the Jimenez deflection model. Since there is no time to study and verify all the wake velocity models in detail the rest of this thesis will mainly stick to the model as described in the previous section combined with rotor tilting as described in the next chapter.

Chapter 4

Extending FLORIS With The Effects Of Turbine Tilt

Currently the FLOw Redirection and Induction in Steady state (FLORIS) model only allows yaw control to be used for wake deflection. In this chapter two wake deflection models will be extended to model the effects of rotor tilting. In the first section the Jimenez deflection model will be extended. In the second section the Bastankhah and Porté-Agel wake deflection model will be extended to include tilt.

4-1 Jimenez wake deflection model with rotor tilting

The reasoning used in [Jiménez et al., 2009] to compute the horizontal wake displacement due to a yaw misalignment can be extended to compute the vertical wake displacement due to a tilt misalignment. This model does expect a uniform flow. However, the windspeed in an Atmospheric Boundary Layer (ABL) varies with height due to the shear layer formed by the ground.

Figure 4-1 shows a turbine that is both yawed and tilted. Currently no turbine exists that allows the tilt angle to be changed actively. This model assumes that the tilting will be implemented at the nacelle. This means it is assumed that the nacelle first yaws and then tilts. (4-1) shows the transformation between the windframe and the rotation that the blades experience.

$$R_T = R_Z R_Y = \begin{bmatrix} \cos(\gamma) & -\sin(\gamma) & 0 \\ \sin(\gamma) & \cos(\gamma) & 0 \\ 0 & 0 & 1 \end{bmatrix} \begin{bmatrix} \cos(\tau) & 0 & \sin(\tau) \\ 0 & 1 & 0 \\ -\sin(\tau) & 0 & \cos(\tau) \end{bmatrix} \tag{4-1}$$

The normalized turbine thrust vector works directly into the wind along the x-axis when there is no rotation. Multiplying this thrust vector with the rotation matrix R_T gives the thrust vector T_d after nacelle rotation.

$$T_d = R_T \begin{bmatrix} -1 \\ 0 \\ 0 \end{bmatrix} \tag{4-2}$$

The thrust vector and wind direction span a plane, indicated in yellow in Figure 4-1. The wake displacement due to turbine rotation as computed in (3-7) happens in this plane. The purple arrow labeled 'Wake direction' spans this plane together with the wind direction. The displacement happens in the direction of the 'Wake direction' unit vector.

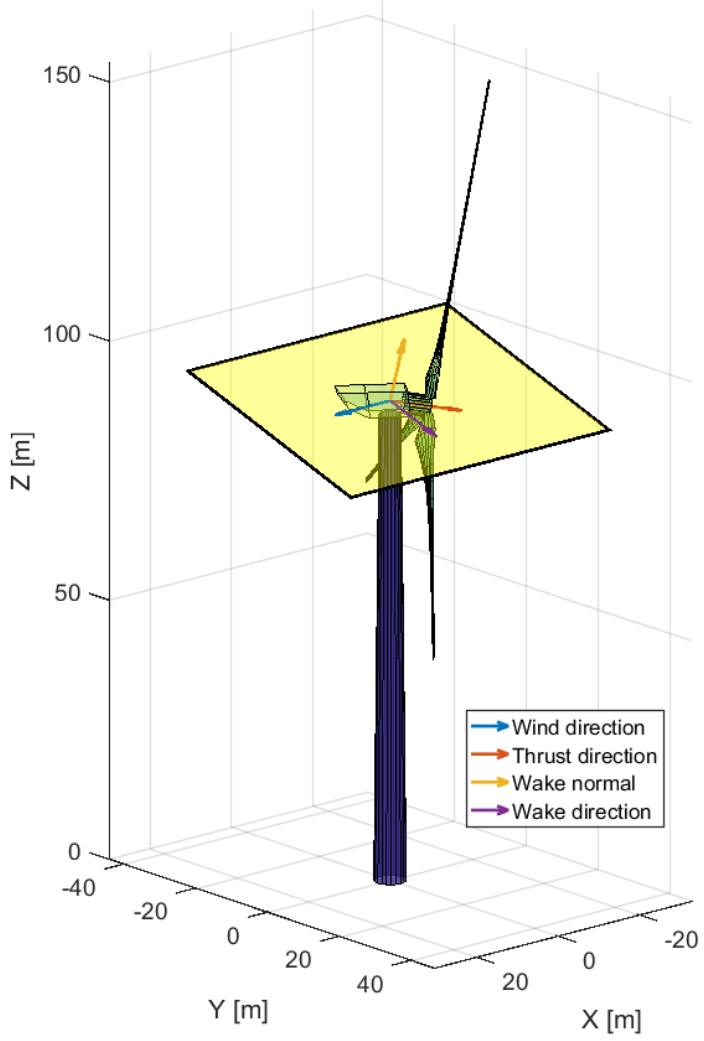

Figure 4-1: Representation of a turbine that is both yawed and tilted

The initial wake angle θ_{init}, as defined in (2-13), is no longer computed using the yaw angle (as was previously done according to Jimenez), but is now instead computed using an angle between the actual thrust vector and the neutral thrust vector as in (4-3). This computation works because all the direction vectors are unit vectors. ψ changes (2-13) to (4-4).

$$\psi = \cos^{-1}(T_d \bullet \begin{bmatrix} -1 \\ 0 \\ 0 \end{bmatrix}) \tag{4-3}$$

$$\theta_{\text{init}}(a, \psi) = \frac{1}{2}\cos^2(\psi)\sin(\psi)C_T(a) \tag{4-4}$$

This new θ_{init} can be used directly in equation (3-7). This formula computes the predicted deflection at some downwind distance x_d as shown in (4-5). This deflection can be multiplied with the vector 'wake direction' from Figure 4-1. The normalized wake direction is shown in (4-6). Since the normalized wake direction W_d only has a y and z component multiplying the deflection with this vector gives the coordinates of the deflected wake centerline.

$$\delta y_{w,rot,i}(x) \approx \frac{\theta_{init}(a_i,\psi_i)\left(15\left(\frac{2k_e(x-X_i)}{D_i}+1\right)^4+\theta_{init}(a_i,\psi_i)^2\right)}{\frac{30k_e}{D_i}\left(\frac{2k_e(x-X_i)}{D_i}+1\right)^5} - \frac{\theta_{init}(a_i,\psi_i)D_i\left(15+\theta_{init}(a_i,\psi_i)^2\right)}{30k_e} \tag{4-5}$$

$$W_d = \frac{T_d[2:3]}{||T_d[2:3]||} \tag{4-6}$$

Now to get the total deflection we should also add the linear expansion shown in (3-8). That formula is based on the results in [Fleming et al., 2014] which shows that a fully wind-aligned turbine has a deflection. This paper shows that there is also a deflection in the z-direction. Because the earlier implementation of FLORIS per [Gebraad et al., 2014] only considered horizontal deflection this was neglected. Now that the model is extended to explicitly compute the wake deflection into the z-direction this deflection can also be taken into account as shown in (4-7).

$$\delta_{\text{total}} = \delta y_{w,rot,i} \cdot W_d + \begin{bmatrix} a_Y + b_Y \cdot x \\ a_T + b_T \cdot x \end{bmatrix} \tag{4-7}$$

4-2 Bastankhah and Porté-Agel wake deflection model with rotor tilting

The Jimenez model only predicts the deflected position of the wake. In the self similar wake model published in [Bastankhah and Porté-Agel, 2016] the wake shape is also dependent on the yaw angle of the rotor. Since this model shows good agreement with measurement data and is grounded in a rigorous theoretical analysis, it would be interesting for this thesis to try and extend it in such a way that it too can capture the effects of a tilted rotor on the turbine wake and power capture. The body of research on the specific effects of turbine tilting is

currently quite small. However the formulation of the Porté-Agel model can be extended to include turbine tilting in a straight forward way.

In the previous section a method is proposed for incorporating turbine tilt in the Jiménez wake deflection model. The method described in that section can also be used to extend the Porté-Agel model with tilt. A rotation matrix R_T was formulated that describes the thrust direction of the rotor (4-1) with τ the tilt angle of the rotor.

Figure 4-3 shows a yawed and tilted turbine, where the red arrow shows the thrust direction of this turbine. The thrust direction is $T_d = R_T \begin{bmatrix} -1 \\ 0 \\ 0 \end{bmatrix}$. The inverse cosine of the dot product between two vectors gives the angle between those vectors, so the thrust angle is $\psi = \cos^{-1}(T_d \bullet \begin{bmatrix} -1 \\ 0 \\ 0 \end{bmatrix})$.

The Gaussian wake velocity model has a potential core whose beginning at $x_d = 0$ is equal to the swept area of the turbine. When both yaw and tilt are applied at the same time a 2by2 matrix is needed to describe the ellipse of the beginning of the potential core. The general formula for an ellipse centered on the origin is shown in (4-8), where $A \in \mathbb{R}^{2\times 2}$ is a matrix describing the size and shape of the ellipse.

$$\begin{bmatrix} y & z \end{bmatrix} A \begin{bmatrix} y \\ z \end{bmatrix} = 1 \tag{4-8}$$

To see how the rotation matrix R_T transforms the front view (the y-z plane) of the turbine, the first row and column can be discarded because these describe the x-components. This leaves just the second and third row and column intersection as a 2by2 matrix. This submatrix of R_T can be used to describe the swept area ellipse of the turbine as shown in (4-9).

$$\begin{aligned} A &= \left(\begin{bmatrix} R_{T_{22}} & R_{T_{23}} \\ R_{T_{32}} & R_{T_{33}} \end{bmatrix} \begin{bmatrix} R & 0 \\ 0 & R \end{bmatrix}^2 \begin{bmatrix} R_{T_{22}} & R_{T_{23}} \\ R_{T_{32}} & R_{T_{33}} \end{bmatrix}^T \right)^{-1} \\ A &= \left(\begin{bmatrix} R & 0 \\ 0 & R \end{bmatrix} \underbrace{\begin{bmatrix} \cos(\gamma)^2 + \sin(\gamma)^2 \sin(\tau)^2 & \cos(\tau)\sin(\gamma)\sin(\tau) \\ \cos(\tau)\sin(\gamma)\sin(\tau) & \cos(\tau)^2 \end{bmatrix}}_{C} \begin{bmatrix} R & 0 \\ 0 & R \end{bmatrix} \right)^{-1} \end{aligned} \tag{4-9}$$

The red ellipse in Figure 4-2 shows the frontal area of a yawed and tilted turbine, it is described by (4-8) and (4-9). The matrix describing the shape of the ellipse is called C. It will also be useful later on in defining the standard deviation of the far wake.

The elliptical frontal swept area of the turbine starts the potential core, the near-wake core vanishes at $x_d = x_0$. This vanishing is described by (4-10). This equation is a variation on the standard ellipse equation as shown in (4-8). Instead of being equal to 1 the quadratic term describing the boundary of the ellipse is equal to the vanishing term $1 - \frac{x_d}{x_0}$. The square

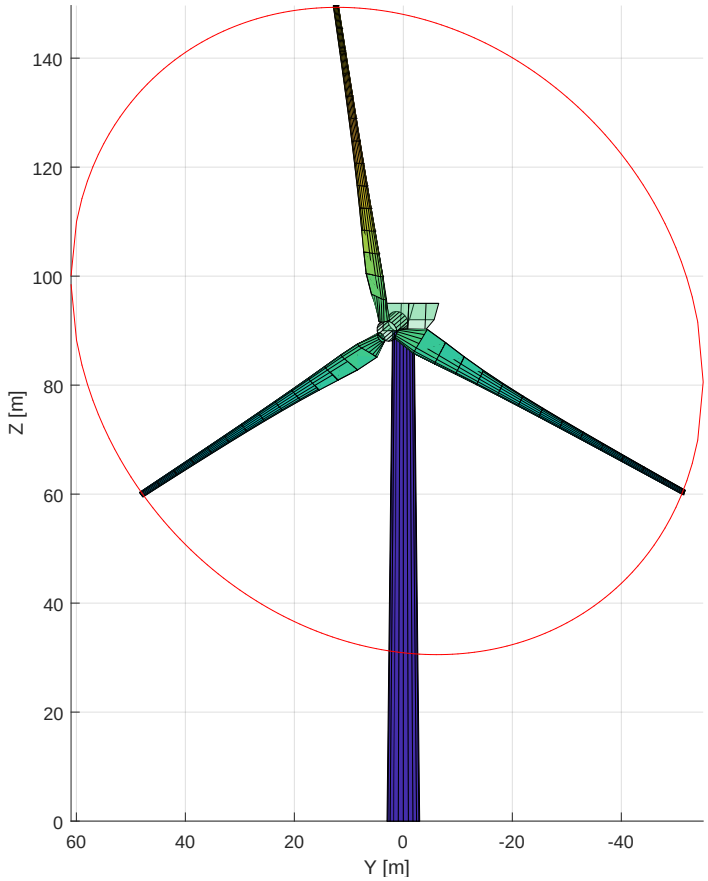

Figure 4-2: frontal swept area of a turbine with $\gamma = 25, \tau = 20$ transforms into an ellipse

root on the left side of the equation is added such that the near-wake core decays linearly instead of quadratically. This is also how the near-wake core is implemented in (3-18).

$$\sqrt{\begin{bmatrix} y & z \end{bmatrix} A \begin{bmatrix} y \\ z \end{bmatrix}} = 1 - \frac{x_d}{x_0} \tag{4-10}$$

Since the model needs to include yaw and tilt a full covariance matrix to describe the Gaussian of the wake is required. Instead of using standard deviations in the y and z direction, C from (4-9) can be used to define that covariance matrix. From (3-17) it can be seen that the standard deviation at x_0 of the wake of a wind-aligned rotor is $\sigma_{z_0} = \sigma_{y_0} = \frac{R}{\sqrt{2}}$. By using these standard deviations the covariance matrix at the onset of the far-wake can be defined as (4-11). Now C changes the standard deviation of the wake in accordance with its yaw and tilt angle. σ_{z_0} and σ_{y_0} are treated as constants in the calculation.

$$\Sigma_0 = \left(\begin{bmatrix} \sigma_{y_0} & 0 \\ 0 & \sigma_{z_0} \end{bmatrix} C \begin{bmatrix} \sigma_{y_0} & 0 \\ 0 & \sigma_{z_0} \end{bmatrix} \right)^{-1} \tag{4-11}$$

Equations (4-10) and (4-11) can be combined to form a description of the near-wake under yawed and tilted conditions. The ellipse ratio, $E_r(x, y, z)$, defined in (4-12), is a term that

determines how much of the distance of some (y, z) point to the wake centerline is part of the core, which is an implementation of $r - r_{pc} = r\,(1 - {}^{r_{pc}}/_{r})$. Equation (4-13) describes how the covariance matrix grows from 0 to Σ_0 over the length of the near wake. Equation (3-18) can now be defined for the tilted case by combining (4-10) to (4-13) into (4-14). This expression fully describes the velocity of the near-wake region of a turbine that is yawed and tilted.

$$E_r(x, y, z) = 1 - \frac{1 - \frac{x}{x_0}}{\sqrt{\begin{bmatrix} y & z \end{bmatrix} A \begin{bmatrix} y \\ z \end{bmatrix}}} \tag{4-12}$$

$$\Sigma_{nw} = \frac{x}{x_0}\Sigma_0 \tag{4-13}$$

$$\frac{V_w}{V_\infty} = \begin{cases} 1 - C_0 & \text{if} \sqrt{\begin{bmatrix} y & z \end{bmatrix} A \begin{bmatrix} y \\ z \end{bmatrix}} \leq 1 - \frac{x}{x_0} \\ 1 - C_0 \mathrm{e}^{-0.5 \begin{bmatrix} y & z \end{bmatrix} \Sigma_{nw} \begin{bmatrix} y \\ z \end{bmatrix} (E_r(x,y,z))^2} & \text{if} \sqrt{\begin{bmatrix} y & z \end{bmatrix} A \begin{bmatrix} y \\ z \end{bmatrix}} > 1 - \frac{x}{x_0} \end{cases} \tag{4-14}$$

Just like in the equations in Section 3-2 y and z always refer to the y and z coordinate with the wake centerline as origin. The x-coordinate is 0 at the turbine. The centerline of the near-wake is again the hypothenuse of a triangle with the starting angle now defined by ψ, the angle of the thrust direction. The expression for the near-wake angle and deflection are shown in (4-15). Notice that this equation is a direct copy of (3-24) but the yaw angle γ has been replaced with the thrust angle ψ.

$$\begin{aligned} \theta_{nw} &= \frac{0.3\psi}{\cos(\psi)} \left(1 - \sqrt{1 - C_T \cos(\psi)}\right) \\ \delta_{nw}(x) &= x \tan(\theta_{nw}) \end{aligned} \tag{4-15}$$

The deflection, δ_{nw}, is in the wake direction as shown by the purple arrow in Figure 4-3. To complete the implementation of turbine tilt, the velocity profile and deflection of the far-wake have to be defined. Equations (3-21),(3-22) and (4-11) can be combined to give an expression for the far-wake variance (4-16).

$$\Sigma_{fw} = \left(\begin{bmatrix} \sigma_y & 0 \\ 0 & \sigma_z \end{bmatrix} C \begin{bmatrix} \sigma_y & 0 \\ 0 & \sigma_z \end{bmatrix} \right)^{-1} \tag{4-16}$$

This expression for the variance combined with (3-23) leads to the velocity profile of the far-wake shown in (4-17).

$$\frac{V_w}{V_\infty} = 1 - \left(1 - \sqrt{1 - C_T \cdot \sqrt{\det(\Sigma\Sigma_0^{-1})}}\right) e^{-0.5 \begin{bmatrix} y & z \end{bmatrix} \Sigma \begin{bmatrix} y \\ z \end{bmatrix}} \tag{4-17}$$

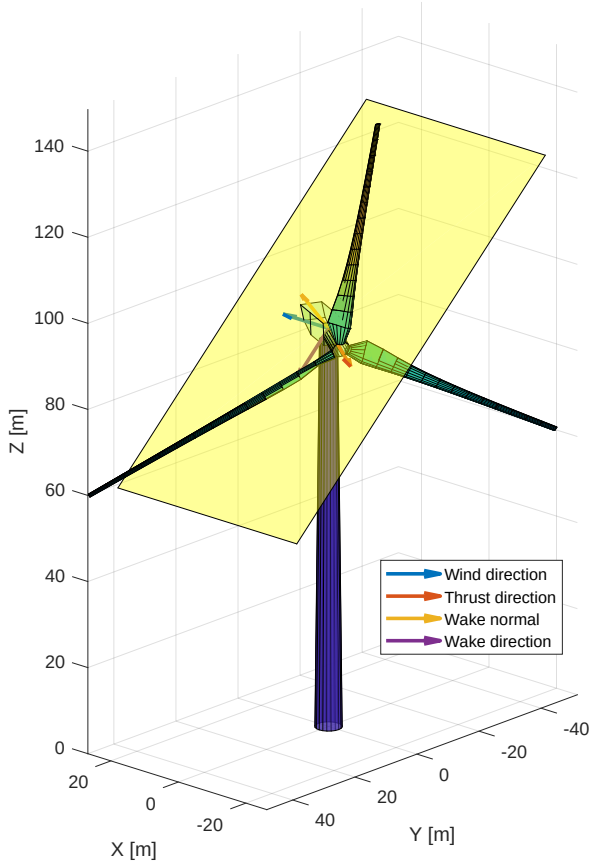

Figure 4-3: thrust direction and other important vectors for turbine with $\gamma = 25, \tau = 20$

Note that in (3-23), the standard deviations at some x and x_0 are divided to describe wake growth. This expression has no direct equivalent in this case since $\Sigma = \begin{bmatrix} \sigma_y^2 & \rho\sigma_y\sigma_z \\ \rho\sigma_y\sigma_z & \sigma_z^2 \end{bmatrix}$ with ρ the correlation between σ_y and σ_z. To correctly implement this division of standard deviations it is still under investigation if the determinant or trace of $\Sigma\Sigma_0^{-1}$ is needed. The results of using the determinant seem to provide better results, using the trace gives an unrealistically slow recovery of the wake. A comparison with high fidelity simulation or experimental data should make clear which method gives more realistic results. This issue also arises when rewriting (3-25) to use a covariance matrix.

$$\begin{aligned} \delta_{fw} = &\tan(\theta_{nw})x_0 + R_t \frac{\theta_{nw}}{7.35}\sqrt{\frac{\cos(\psi)}{k_y k_z C_T}}\left(2.9 + 1.3\sqrt{1-C_T} - C_T\right) \\ &\times \ln\left[\frac{\left(1.6+\sqrt{C_T}\right)\left(1.6\sqrt[4]{\det(\Sigma\Sigma_0^{-1})} - \sqrt{C_T}\right)}{\left(1.6-\sqrt{C_T}\right)\left(1.6\sqrt[4]{\det(\Sigma\Sigma_0^{-1})} + \sqrt{C_T}\right)}\right] \end{aligned} \tag{4-18}$$

As described in Subsection 3-2-3 the turbine rotation induced wake deflection is not yet

accounted for and should be added. This can be done by combining similar to (3-26) and (4-7), the final result is shown in (4-19).

$$\delta_{\text{total}} = \begin{cases} \delta_{nw} \cdot W_d + \begin{bmatrix} a_Y + b_Y \cdot x \\ a_T + b_T \cdot x \end{bmatrix} & \text{if } x \leq x_0 \\ \delta_{fw} \cdot W_d + \begin{bmatrix} a_Y + b_Y \cdot x \\ a_T + b_T \cdot x \end{bmatrix} & \text{if } x > x_0 \end{cases} \tag{4-19}$$

Chapter 5

Model Parameter Estimation

In the previous chapter an extension to the FLOw Redirection and Induction in Steady state (FLORIS) model was proposed that does not add any new fitting parameters. However, the accuracy of the model is dependent on the specific model parameters that are used. The nominal model parameters that are currently used are all based on a very limited amount of studies and none of those studies have published confidence intervals on those parameters. This is true for every submodel of the FLORIS model. Even though the rotor tilting extension does not require new fitting parameters, a structural method to determine the fitting parameters is necessary for confidence in the model. The main criteria for a good fit is accurate time-averaged power prediction for a range of wind-farm operations. It is expected that the flow predictions of the far wake will need to match reality as closely as possible for the power to be accurately predicted. Therefore, increasing the FLORIS fit on flow data should also increase its power prediction accuracy.

A general problem in parameter estimation is overfitting. Overfitting usually happens when many model parameters are tuned on a small dataset, resulting in the model predicting that small dataset very well but giving poor results on other data. In short, overfitting refers to the situation where a good fit is achieved on some training data but the model fails to generalize to other situations. One of the main strategies to prevent overfitting is to increase the amount of training data. This can and will be applied to FLORIS as well. Another strategy is to reduce model complexity. Because FLORIS is already a simplified model, we will attempt something slightly different. We propose a method to identify situations in which only certain parameters of the model are sensitive. The sensitivity of a model parameter is loosely defined as the magnitude of the change in the output power when that model parameter is varried. Thus, identifying situations where some parameters are not sensitive allows these parameters to be held constant during parameter optimization since they are not sensitive. This is effectively the same as reducing model complexity. The word 'situation' will be used throughout this chapter and it refers to a combination of four factors.

1. turbine positions in the wind farm,
2. wind speed,

3. wind direction, and
4. atmospheric turbulence.

These four factors have a big influence on the sensitivity of the model and they are better thought of as external inputs than as model parameters.

One of the main ideas in the fitting procedures is identifying situations in which only some parameters are sensitive. To assist this search, the next section discusses the effects that all model parameters have on predicted power and flow characteristics. This discussion is also a more general description of the behaviour of FLORIS. It will allow us to reason about the expected behaviour while changing parameters and determine if the model is behaving correctly or not. After that discussion, a sensitivity analysis is presented in the following section. That sensitivity analysis starts with a One At a Time (OAT) analysis.

The idea in an OAT analysis is to vary one input variable, keeping others at their nominal values. Then, the variable is returned to its nominal value and the procedure is repeated for all other variables. The most important choice made in this type of analysis is the range each variable should vary in. A good approach is to vary each parameter within it's own 95% confidence interval. This will determine how large a variable's effect on the power production is likely to be.

Quantifying these ranges is difficult, because none of the original papers on which FLORIS is based published confidence intervals on their nominal parameter values. All of the parameters are fitted to a certain amount of high-fidelity Computational Fluid Dynamics (CFD) data or either small-scale or full-scale experimental data. Because there are no confidence intervals available, every parameter will simply be halved from its nominal value in literature to get a lower bound, and doubled to get an upper bound. This is quite arbitrary, but it will serve as a starting point. The resulting behaviour of FLORIS and the effects on the predicted power production are analyzed in detail in the next subsections.

5-1 Parameter Effects On Power And Flow Predictions

The FLORIS model includes several wake models, each of which has their own set of fitting parameters. For brevity, the sensitivity analysis in this work is focused on the FLORIS model as described in Section 4-2. This refers to the Gaussian wake model and the Bastankhah and Porté-Agel wake deflection model with rotor tilting. The parameters can be loosely grouped in four sets. These sets form a suitable starting point for this analysis. Parameters α and β, first explained in (3-12), both affect the length of the near-wake core. Parameters k_a and k_b control the wake expansion as shown in (3-19). The other two parameter sets are the turbulence fitting parameters, I_a, I_b, I_c and I_d, and the wake displacement bias parameters, a_Y, b_Y, a_T and b_T.

There is no hard rule dividing these parameter sets, but since they all affect distinct parts of the model, it is a good starting point for discussing how each of them affects the model behaviour. The next four subsections discuss these four parameter sets.

It is important to keep in mind throughout the discussion that none of these model parameters directly affect the power production. The only way these parameters affect the power

production is by shaping the wake, and thereby affecting the wind conditions at down wind turbines. This is a basic property of the FLORIS model and it applies to all its variants. It is also the main reason that the sensitivity is so dependent on the situation, i.e., the four points mentioned in the introduction.

5-1-1 Near-wake core parameters

The length of the near-wake core, x_0, is given by (3-12) and repeated here for clarity:

$$x_0 = \frac{\sqrt{2} \cdot R \cdot \cos(\gamma)(1 + \sqrt{1 - C_T})}{\alpha \cdot I + \beta(1 - \sqrt{1 - C_T})} \tag{3-12}$$

Both α and β are negatively correlated with x_0. α modulates the impact that turbulence intensity, I, has on the core length and, β determines how much effect the thrust coefficient, C_T, has on core length. Increasing either parameter will thus decrease the near-wake length. A shorter near-wake core means a quicker decay of the wake and thus a higher effective inflow velocity at the downstream turbine rotors. Thus we expect that increasing either parameter will have a positive effect on the total power production. The current nominal values are $\alpha = 2.32$ and $\beta = 0.154$. These values are proposed in [Bastankhah and Porté-Agel, 2016]. The following paragraph is a short summary of the relevant parts of that paper.

The value of β is based on research done on jet flow studies. In those studies β, is estimated by making an experimental setup with laminar flow e.g. $I = 0$. The value found for β in those studies is in good agreement with small-scale experimental wind turbine data. Next, the near-wake core length was estimated from measurements made during four yaw angles and two tip-speed ratios and $I \approx .07$. α is then fitted in such a way that (3-12) corresponds well to these eight test cases. For more details on the exact experimental setup, see [Bastankhah and Porté-Agel, 2016]. A good fit arises, but these are now only based on small-scale measurements. Fitting the parameters on full-scale wind turbine flow, either experimentally or computationally, will likely change the parameter estimates.

α and β modulate the effect that the turbulence intensity, I, and thrust coefficient, C_T, have on the near wake core-length. This means that the situations used to tune these parameters at least require non-zero I and C_T. Preferably, the parameters should be tuned for a range of turbulence intensities and thrust coefficients that the model would typically encounter in a wind farm. Doubling and halving the nominal values to get the optimization boundaries results in:

- $1.16 < \alpha < 4.64$
- $0.077 < \beta < 0.308$

5-1-2 Expansion parameters

In the Porté-Agel model the wake-profile is described using a 2D Gaussian function. The relevant equations are repeated here for clarity. The standard deviations in the lateral and vertical direction, σ_y and σ_z, both grow linearly with downwind distance as shown in (3-21)

and (3-22). The wake growth parameters k_z and k_y are in turn linear functions of turbulence intensity (3-19). It is possible to have different growth rates for the different axes, but currently they are taken to be equal in accordance with [Bastankhah and Porté-Agel, 2016].

$$k_z = k_y = k_a I + k_b \tag{3-19}$$
$$\sigma_z = \sigma_{z_0} + (x - x_0) \cdot k_z \tag{3-21}$$
$$\sigma_y = \sigma_{y_0} + (x - x_0) \cdot k_y \tag{3-22}$$

σ_{z_0} and σ_{y_0} are the standard deviations of the wake on the boundary between the near and far wake. The downwind distance from the turbine is denoted by x and x_0 is the start of the far wake. The relevant fitting parameters for the far wake expansion are k_a and k_b. An increase in either parameter will cause the wake to expand, and thus decay, quicker. This should lead to an increase in the power production of downwind turbines. Both wake expansion parameters have a positive correlation with power production. There can be some niche situations where a turbine is positioned just outside of the wake, and increasing k_a or k_b would put the turbine just within reach of a wake. This would only lead to a small decrease in power because the flow near the outer edge of a wake is almost equal to the freestream. Still, this situation demonstrates that tuning these parameters is very dependent on the specific turbine positioning. Parameter tuning on a too narrow dataset both in terms of turbine positioning and turbulence intensities could worsen the power predictions of FLORIS instead of increasing the accuracy.

The current nominal values for k_a and k_b are 0.3837 and 0.003678, respectively. These values are based on Large Eddy Simulation (LES) simulations of a V80-2MW turbine [Bastankhah and Porté-Agel, 2014]. The linear function is fitted on turbulence intensities ranging from .065 to .15 since these are typical atmospheric values [Göçmen and Giebel, 2016]. Further research and simulations for a wider range of turbulence intensities might suggest different fitting parameters. Maybe the linear relationship itself will not hold when a wider range of turbulence intensities is considered. Doubling and halving the nominal values results in:

- $0.192 < k_a < 0.767$
- $1.84 \cdot 10^{-3} < k_b < 7.36 \cdot 10^{-3}$

5-1-3 Turbulence parameters

As explained in the preceding sections, the turbulence intensity at a rotor affects the length of its near-wake core and changes the decay rate of its wake. Wind turbines generate additional turbulence in their wakes since there are multiple turbine blades disturbing the flow. The added turbulence caused by some wind turbine k is defined as I_k^+. The total turbulence at the rotor of a downwind turbine is computed by taking the euclidean norm of the atmospheric turbulence and the added turbulence of each wake that partially overlaps the rotor. The equation for this is repeated here for clarity, (3-15)

$$I = ||\frac{A_1}{A} I_1^+, \cdots, \frac{A_n}{A} I_n^+, I_0|| \tag{3-15}$$

There are several models that can be used to estimate the added turbulence intensity I_k^+, three of which are described in [Niayifar and Porté-Agel, 2015]. The added turbulence model used by Bastankah and Porté-Agel in[Bastankhah and Porté-Agel, 2016] is shown in (3-13). This expression is originally proposed in [Crespo and Hernández, 1996]. In this model, the added turbulence intensity I_k^+ depends on the axial induction a, atmospheric turbulence I_0 and relative downwind distance x/D. The relative downwind distance is the downwind distance from the rotor x divided by the rotor diameter D. The fitting parameters of the added turbulence model are I_a, I_b, I_c and I_d. The atmospheric turbulence, I_0, is not a fitting parameter but has to be derived from measurements just like wind direction and wind velocity.

$$I_k^+ = I_a a^{I_b} I_0^{I_c} (x/D)^{I_d} \tag{3-13}$$

The current numerical values $I_a = .73$, $I_b = .8325$, $I_c = -.0325$ and $I_d = -.32$ are proposed in [Crespo and Hernández, 1996]. The numerical values are a least square fit on CFD data computed using the UPMWAKE model which is based on Reynolds-Averaged Navier-Stokes (RANS) equations. In the original paper [Crespo and Hernández, 1996], it is not clear what turbines or wind farm layout were used to generate results. The parameter ranges that were used to estimate the fitting parameters were specified in the paper:

- $0.07 < I_0 < 0.14$
- $5 < x/D < 15$
- $0.1 < a < 0.4$

The turbulence intensity range matches closely to the $.065 < I_0 < .15$ range used in the tuning of the wake expansion parameters. Again, outside this range we cannot know if the relationship holds and if the numerical values are valid. The distance range excludes the first five blade diameters, which corresponds approximately to the near-wake region. Thus when tuning parameters other than the turbulence parameters, care should be taken to avoid this uncertain region. Thus, for any parameter tuning datasets should be used that do not have downwind turbines positioned within 5D. This holds as a more general rule, because analytical wake models tend to be inaccurate when modeling the near wake [Charhouni et al., 2015]. The axial induction covers a wide range of practically encountered scenarios, as explained in Section 2-1, $a = 0.0$ would mean no energy extraction. And $a = 0.5$ would mean a physically perfect extraction of wind energy which is not practically achievable with current wind turbines.

A problem with tuning the fitting parameters, I_a, I_b, I_c and I_d, is that the added turbulence only affects the total power production if there is a turbine array of at least three turbines deep. To make this clear, think of it like this: The added turbulence model has no effect on the first turbine, only the atmospheric turbulence intensity does, but that is not a model parameter. The added turbulence has no effect on the second turbine's power production either; it only changes its wake. Then finally those wake changes have an effect on the power production of a third turbine. If the turbulence parameters are tuned on power data, that data should be selected carefully such that it is mostly sensitive to changes in the turbulence

parameters. It might be better to try and fit the added turbulence parameters on measured or modeled flow information instead of fitting on power information.

Now that most caveats of the added turbulence model have been explained, what remains in this section is to investigate how the individual model parameters affect the turbine induced added turbulence, I_k^+. An increase in I_a or a has a positive correlation with the added turbulence and thus a positive correlation with predicted power. Since a is always between 0.0 and 0.5, increasing the value of it's exponent, I_b, decreases added turbulence. Therefore, I_b is negatively correlated with power production. Likewise, the atmospheric turbulence, I_0, is always between zero and one. This means that decreasing the fitting parameter I_c increases the added turbulence. Note that the atmospheric turbulence, I_0, itself is not a fitting parameter. A larger I_0 actually decreases the added turbulence. An explanation for this effect is that, if the air is already turbulent, a turbine blade swinging through it is going to make a smaller difference on the total turbulence at some downstream location x. The last turbulence fitting parameter, I_d, is the exponent of x/D the relative downwind distance from the turbine. The model is only valid if the downwind distance is larger than five rotor diameters. Thus, if I_d grows, the added turbulence and the predicted power grow as well.

The numerical values proposed in [Crespo and Hernández, 1996] do not seem to have been verified by other researchers. The confidence in the results of the equation is strong enough for it to have been published in several papers. Taking optimization boundaries as double and halve the nominal values for all four turbulence fitting parameters results in:

- $0.365 < I_a < 1.46$
- $0.416 < I_b < 1.67$
- $-0.065 < I_c < -0.0163$
- $-0.64 < I_d < -0.16$

5-1-4 Deflection parameters

The wake deflection as proposed in [Bastankhah and Porté-Agel, 2016] is an analytical expression without fitting parameters. The effects of blade rotation on the wake are discussed initially but are eventually omitted for simplicity. This leads to the wake deflection being zero when the turbine is unyawed. Earlier studies show the unyawed case should have a deflection [Fleming et al., 2014] and [Fleming et al., 2015]. This blade-rotation-induced wake deflection can be fitted using a linear function [Gebraad et al., 2014]. Thus, the Porté-Agel model used in FLORIS has been extended in a similar fashion with two linearly fitted functions for both the lateral and vertical wake displacement as explained in Section 4-2 and shown in (4-19) and repeated here for clarity.

$$\delta_{\text{total}} = \begin{cases} \delta_{nw} \cdot W_d + \begin{bmatrix} a_Y + b_Y \cdot x \\ a_T + b_T \cdot x \end{bmatrix} & \text{if } x \leq x_0 \\ \delta_{fw} \cdot W_d + \begin{bmatrix} a_Y + b_Y \cdot x \\ a_T + b_T \cdot x \end{bmatrix} & \text{if } x > x_0 \end{cases} \tag{4-19}$$

The four fitting parameters for the blade-rotation-induced wake deflection are a_Y, b_Y, a_T and b_T. The Y subscript denotes the yaw parameters and T the tilt parameters. The effect of these parameters on power prediction is always dependent on the wind farm layout. Deflecting a wake will cause it to overlap either more or less dependent on the relative downwind position of the next turbine.

The values currently used are $a_Y = -4.5$, $b_Y = -0.01$ and $a_T = b_T = 0$. The tilt deflection parameters are currently set to zero in alignment with existing models which only model the deflection in horizontal plane. The tilt parameters, a_T and b_T, are expected to be smaller than the yaw parameters since the rotation-induced displacement is stronger in the lateral direction than the vertical direction [Fleming et al., 2014]. The current values for the yaw fitting parameters are identical to those used in [Gebraad et al., 2014], since the same NREL 5MW turbine model is assumed.

These parameters have a strong and non-linear dependence on the wind farm layout. This should be kept in mind when selecting situations to tune the parameters. The sign of these fitting parameters will also change when the model is used for turbines with a counter clockwise blade rotation. Instead of halving and doubling the tilt parameters, they will be given the same optimization boundaries as the yaw parameters. As stated before the required interval to find good parameters is probably smaller since the deflection effect is smaller in the z-direction. However, from the paper [Fleming et al., 2014] it is not entirely clear if the vertical blade rotation induced deflection is positive or negative. And since there is no preliminary fit the uncertainty is greater. As optimization boundaries for the tilt parameters, $\pm$ the upper boundaries of the yaw parameters will be taken. Taking the optimization boundaries for the yaw parameters to be double and half the nominal values found in [Gebraad et al., 2014] results in:

- $-9.0 < a_Y < -2.25$
- $-.02 < b_Y < -.005$
- $-9.0 < a_T < 9.0$
- $-.02 < b_T < .02$

5-2 Isolating parameters

The previous section discussed how the model parameters affect the flowfield and power production. Most of the effects are in some way dependent on the specific situation for which FLORIS is used. Recall that the term situation refers to the layout of the wind farm, atmospheric turbulence intensity and the wind direction and magnitude. This poses an unusual problem for this sensitivity analysis. When doing an OAT analysis, a Monte Carlo simulation or a similar investigation, the results alone do not convey enough information. The results of any such sensitivity analysis should always be placed in the context of the situation in which they have been gathered. Changing the situation will change the sensitivity. This means that we have to develop some figures that display the situation and the sensitivity at the same time and graphs that show how the sensitivity changes with changing situations.

An interesting point from the discussion in the preceding section is that only the turbulence parameters require a turbine array of at least three turbines deep. The effects of the other parameters should also be visible with just two consecutive turbines. This means that tuning the turbulence parameters has to happen in wind farms with at least three rows of turbines, other model parameters might be tuned on just a two turbine setup. In the next section, these dependencies will be exploited in order to identify situations for which a set of parameters can be tuned.

5-2-1 OAT analysis

An OAT analysis is used to determine the effect that varying one model parameter has on the predicted power. The parameter is changed from its nominal value to a higher value and then to a lower value. The model is simulated in each case and the change in power prediction is recorded. The predicted power can never be completely accurate and this analysis gives insight into what parameters contribute most to the prediction uncertainty. The results of an OAT analysis are usually graphed using a tornado plot. Figure 5-1 shows an example tornado plot of FLORIS.

The figure shows the baseline power generation as 13.1MW, and it shows how the predicted power changes when a single model parameter is changed to its high and low value. The name tornado plot refers to the shape when all the bars are ordered on length. However in this case the parameters are ordered such that they correspond to the parameter sets as discussed in section 5-1. The high and low values listed in that section are also the high and low values used to generate plots in this section.

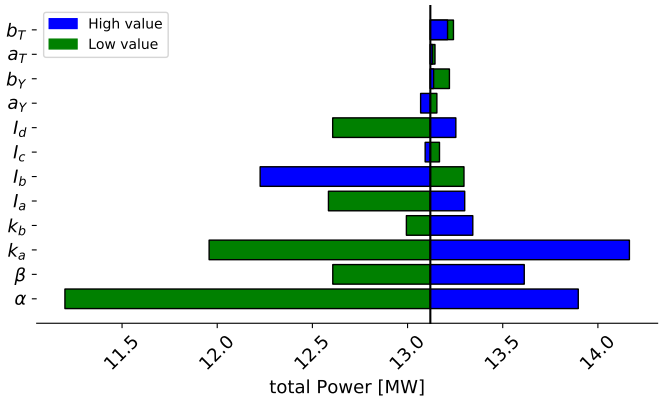

Figure 5-1: Tornado plot of 9 turbines with U = 8m/s, $I_0 = .06$ and $U_{dir} = 0°$

The conditions used to generate this plot are listed below the graph. However, the tornado plot does not convey any information about the layout of the wind farm. The layout has important effects on the power production and its sensitivity. For this reason, every tornado plot will be combined with a contour graph of the flowfield as shown in Figure 5-2.

The first thing to investigate is the effect of wind farm size on the relative importance of the model parameters. A typical is used windspeed, $U_\infty = 8$m/s, in combination with a typical atmospheric turbulence, $I_0 = .06$, and a wind-direction of $U_{dir} = 0°$ to ensure overlapping wake effects. The spacing between the turbines is eight rotor diameters in the wind-aligned

and seven in the cross wind frame. The spacing between the turbines is chosen such that turbines are not positioned in the near wake area, since velocity predictions in that region are in general not reliable.

This atmospheric condition was used to simulate a wind farm for ten different sizes, varying from a 2x2 layout to an 11x11 layout. The resulting plots corresponded to the predicted effects quite well. From 2x2 until 6x6 the relative sensitivity of the parameters varied. The windfarms with a 6x6 until an 11x11 layout had very similar tornado plots meaning that the parameters had the same relative importance. The results for the 6x6 windfarm are shown in Figure 5-2.

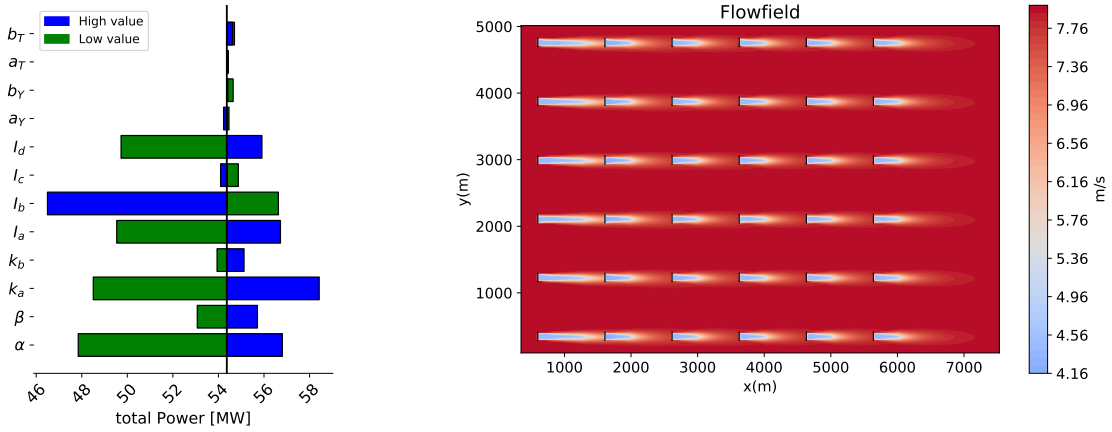

Figure 5-2: Tornado plot and flowfield of 36 turbines with U = 8m/s, $I_0 = .06$ and $U_{dir} = 0°$

The tornado plot on the left hand side of Figure 5-2 is similar in larger wind farms at least up to 11x11. It is likely that the similarity holds for windfarms larger windfarms as well. However, there might be unforeseen behaviour in the model that will change the sensitivity when the wind farm grows even further. One of the first thing to notice is that the added turbulence model has a large effect on the model uncertainty. Three out of the four turbulence parameters, namely I_a, I_b and I_d, have large effects. Their importance in this situation is compounded because of the low atmospheric turbulence of $I_0 = .06$. It is also noticeable that the deflection parameters, a_Y, b_Y, a_T and b_T, have only a small effect. This is to be expected since the blade rotation induced deflection is small, at $7D$ downwind the horizontal deflection is around $0.08D$ [Fleming et al., 2014].

To tune the deflection parameters, it should be possible to formulate a situation with only two turbines that are sensitive to the deflection parameters. This can be done by moving the downwind turbine around experimentally or in a simulation and then analyzing the power production at different locations. Analyzing the flowfield of one turbine can also be a good route to determine the expected deflection parameters. This approach will be further explored in subsection 5-2-2.

Accurately determining the turbulence parameters will require more than two turbines. This is due to the turbulence only affecting wake length and not power production. Thus, added turbulence can only influence the power production of a third turbine as described in subsection 5-1-3. The next step is using the 6x6 wind farm to try finding a situation where the turbulence parameters account for most of the uncertainty.

The inflow in the 6x6 windfarm will be rotated 360 degrees and each parameter will again be varied in an OAT fashion. The results are graphed in a polar plot for each parameter. This is shown in Figure 5-3. These polar plots all have three lines depicting the low, nominal and high value for each parameter. These values are identical to the ones used to generate the previous figures.

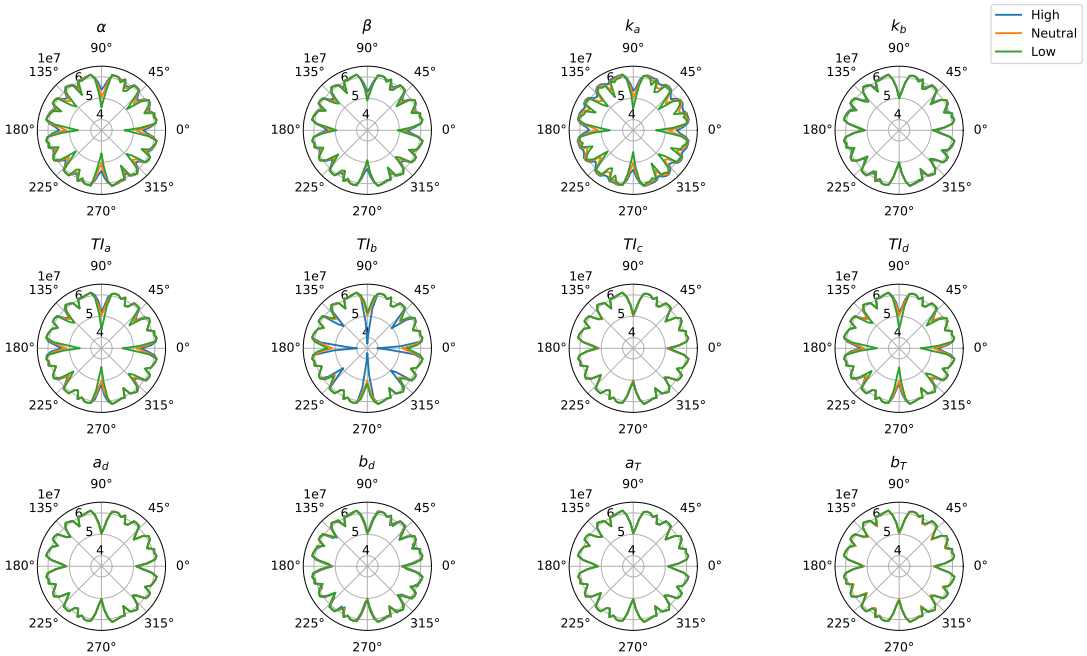

Figure 5-3: Polar tornado plot for 36 turbines

In the polar plot we can see that the turbulence parameters have the biggest effect at a wind-direction of 0° and 90°. But when plotting the tornado plots for these wind-directions, it is clear that the near-wake length and expansion parameters also account for a large portion of the variance. This is show in Figure 5-4.

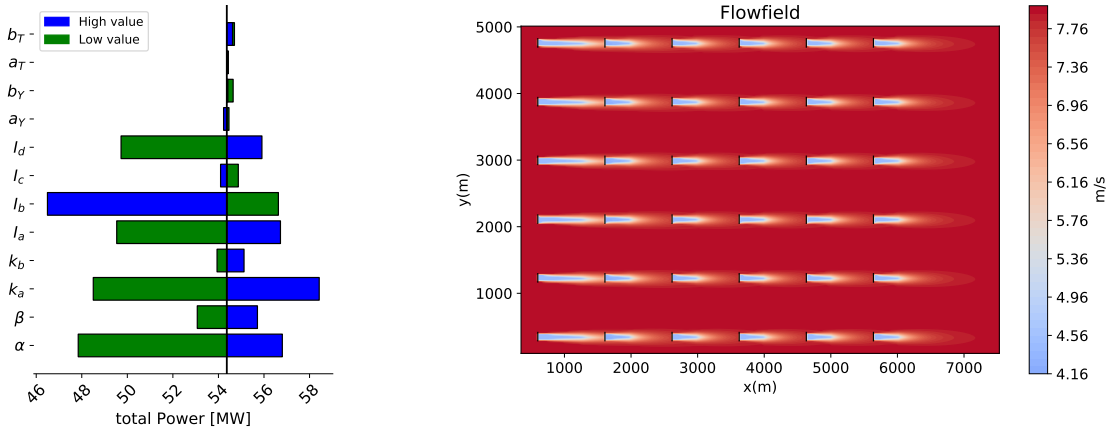

Figure 5-4: Tornado plot and flowfield of 36 turbines with U = 8m/s, $I_0 = .06$ and $U_{dir} = 5°$

In both situations the turbines and their wakes are both completely wind-aligned. Tuning just

the added turbulence parameters and leaving out α, β, k_a and k_b will likely lead to overfitting the added turbulence parameters. This means that the added turbulence try to reduce fitting errors which are actually caused by the expansion and near-wake length parameters. Maybe it is possible to find a situation in which the turbulence parameters have a minimal impact on the model but these four parameters still do. Then, we can tune those parameters first and tune the remaining model parameters under different situations.

When looking at Figure 5-3, there seems to be a situation at 22.5° where the added turbulence parameters show almost no sensitivity. The expansion and near-wake core parameters do however still show some variance. The tornado plot for this situation is shown in Figure 5-5.

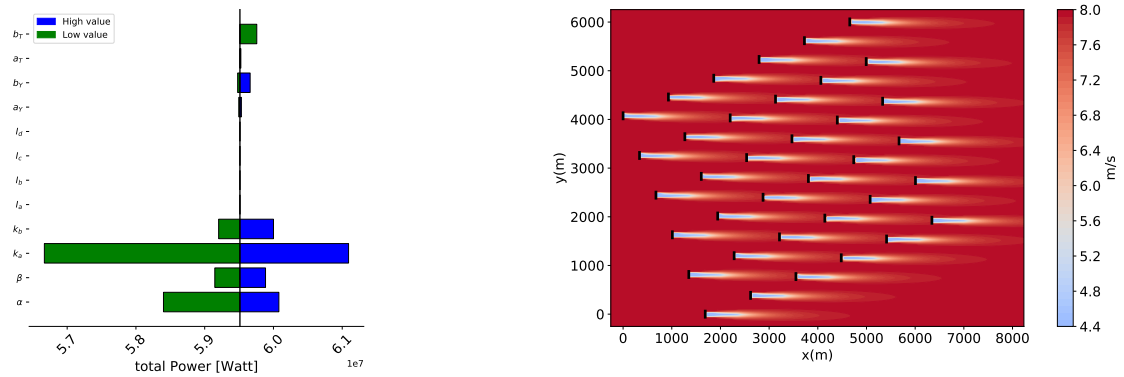

Figure 5-5: Tornado plot and flowfield of 36 turbines with U = 8m/s, $I_0 = .06$ and $U_{dir} = 5°$

Now it is possible to accurately tune FLORIS. Start by tuning the deflection parameters on a situation with only one or two turbines. The effect of a_Y, b_Y, a_T and b_T is not very large but they have an important role, especially when there are fewer wind turbines. After the deflection parameters are tuned, tune the expansion and near-wake core length parameters. Lastly fit the turbulence parameters.

Due to lack of time, no high-fidelity simulations are performed that would be necessary for the tuning of the entire FLORIS model, as described in this chapter. Rather, to demonstrate how it should work the next section will show how to fit the deflection parameters on a two turbine setup.

5-2-2 Tuning the deflection parameters

As mentioned earlier, the wake deflection parameters can be tuned on a two turbine setup. This means running Simulator for Onshore/Offshore Wind Farm Applications (SOWFA) simulations with two turbines for a number of cases and fitting the deflection parameters to minimize some error metric. To reduce the amount of simulations that has to be run in SOWFA we used a shortcut. We simulated a single turbine with different control settings and used the resulting flowfield to compute the power production of a second imaginary turbine. The turbine control settings are the blade pitch, nacelle yaw and rotor tilt.

Each simulation ran for 600 seconds and a time averaged 3D flow-field of the last 300 seconds was generated. The grid has an element size of $10m^3$ and is 3250m in the stream-wise direction, 1600m wide and 300m high. This flow-field was then used to compute the power production of

an imaginary second turbine placed somewhere downstream. This second turbine is identical to a turbine used in FLORIS but uses the flowdata from SOWFA as its input instead of flowdata from FLORIS.

Figure 5-6 shows the combined power production of the simulated SOWFA turbine and the virtual FLORIS turbine. The virtual turbine is positioned at five and ten rotor diameters downstream. The downwind turbine is than shifted along the y-axis from -300 meters to +300 meters. These exact scenarios are then also computed using FLORIS and both predictions are plotted in the same graph.

The red lines depict the combined turbine power at five diameters downstream and the blue lines show the power production at ten diameters downstream. Furthermore, the thick lines are based on the SOWFA data while the thinner lines are pure FLORIS simulations. The dashed lines are off-nominal parameter settings for the deflection parameter a_d.

The four subfigures are all based on a different SOWFA simulation with different control settings. All the figures have zero bladepitch. The top-left figure has neutral wake steering settings. Both the yaw and the tilt angles are zero. The top right figure has a positive tilt angle. And the bottom figures have a positive and negative yaw angle respectively.

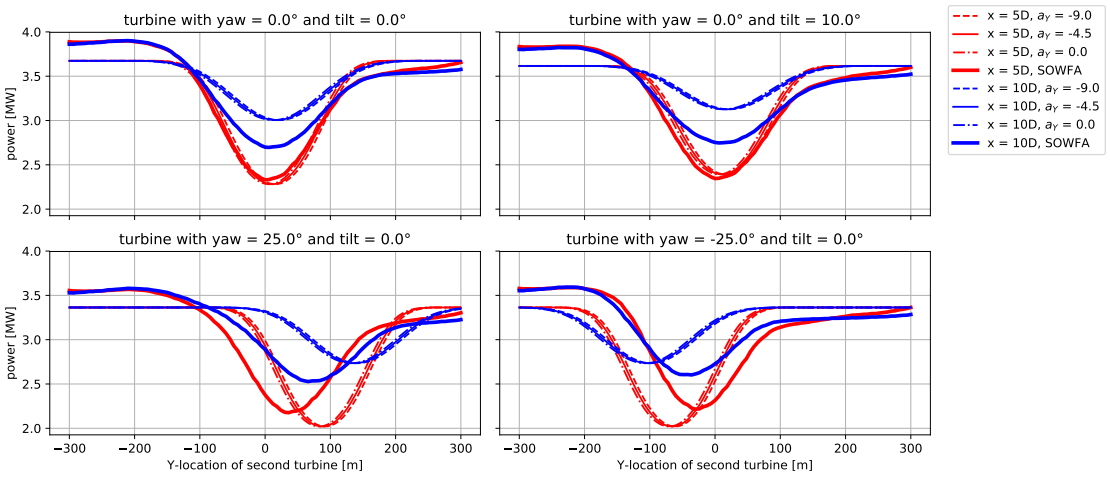

Figure 5-6: Power production of two turbines with second turbine at $\Delta x = [5D, 10D]$ and $\Delta y = [-300 : 5 : 300]$. Four different turbine control settings were used on the first turbine.

The first thing to notice about the figures is that both FLORIS and SOWFA predict a lower power production when the second turbine is positioned in the wake. This is the drop in the middle of each graph around $\Delta y \approx 0$. A problem occurring in all four situations is that power prediction of the second turbine grows worse when it is positioned further downstream. This means that either the atmospheric turbulence intensity of FLORIS does not accurately match the SOWFA simulation, or that the wake decay prediction of FLORIS is not properly tuned to the atmospheric turbulence intensity. Either way the predictions match better around 5D downstream.

Another noticeable difference between SOWFA and FLORIS in this case is that the SOWFA data predicts a much higher power production on the left of the wake, which is surprising. Checking the wind speeds at the second virtual turbine shows that the turbine at $\Delta y = -300$m has an average wind-speed of around 8.15m/s at the rotor. The turbine at $\Delta y = +300$m has

an average wind-speed of 7.85m/s at the rotor. This is all that is needed to get such large deviations in predicted power. This small velocity difference seems to be an artificat of the recursor that occurs in all the simulations independent of their control settings.

One more observation is that at yaw angles as large as $\pm 25°$ the wake deflection is over-predicted by the Porté-Agel model/FLORIS. The SOWFA results show decidedly less yaw-induced deflection than FLORIS is predicting. The power predictions of both simulations relative to the wake displacement are however quite accurate. This is not important for tuning the deflection parameters since that should be done on an un-yawed and un-tilted situations as shown in the top left subfigure.

At the top left figure, the SOWFA and FLORIS predictions match at the 5D distance. This means that the original fitting parameters are good enough for now. Trust in these parameters could be increased by fitting these lines when the CFD has been generated with different precursors. After the wake decay parameters have been fitted this figure should also be reproduced to check if the blue lines do indeed match better.

Now to tune the tilt deflection parameters, a_T and b_T, we will make a similar plot but with the turbine shifting 25 meters up and down at 5D and 10D. We expect the un-yawed and un-tilted situation plotted in the top left to be slightly off while the other cases show a large deviation to due other inaccuracies related to their controls settings. The graphs are shown in Figure 5-7.

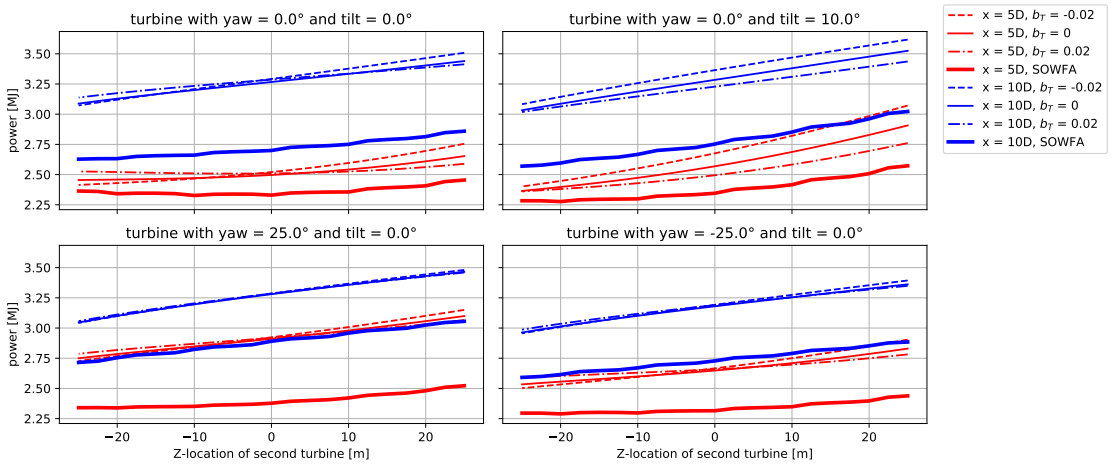

Figure 5-7: Power production of two turbines with second turbine at $\Delta x = [5D, 10D]$ and $\Delta z = [-25 : 2 : 25]$. Four different turbine control settings were used on the first turbine.

The match between the parameter baseline, e.g. $a_T = 0$ and $b_T = 0$, and the SOWFA simulation is indeed good in the top left case. The SOWFA power falls just within the chosen range for the parameter. We will optimize a_T and b_T simultaneously by minimizing the Root Mean Sqaure (RMS) between the FLORIS and SOWFA prediction. The resulting parameter values are $a_T = -7$ and $b_T = .0179$. The un-yawed un-tilted figure is reproduced in Figure 5-8 with these new parameters.

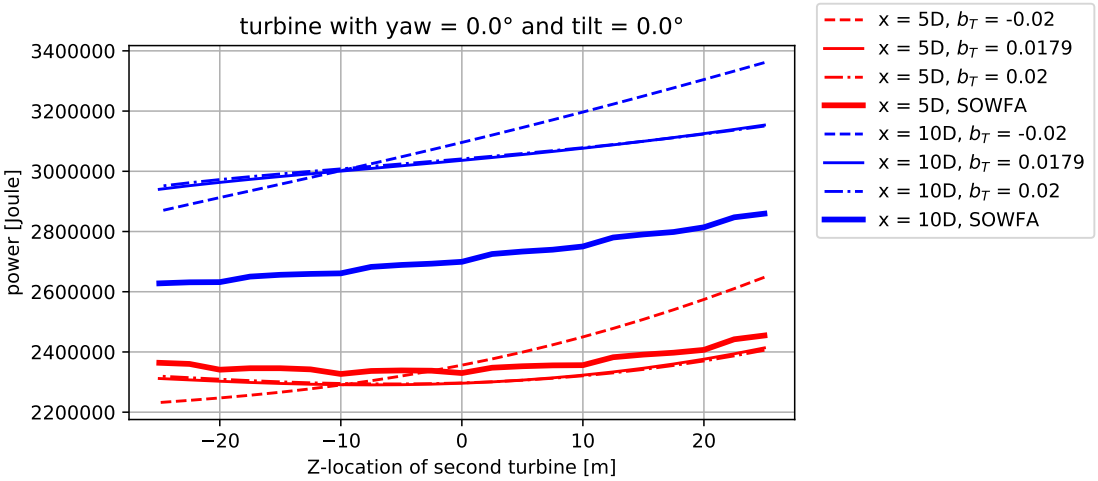

Figure 5-8: Power production of two turbines with second turbine at $\Delta x = [5D, 10D]$ and $\Delta z = [-25 : 2 : 25]$. New fitted deflection parameters.

The power match is not exact and more data is needed to have any confidence in those parameters. The power prediction at 10D downstream is also still off by 0.4[MJ] but this should be improved by tuning the wake expansion parameters and the turbulence intensity parameters. The proper way to tune these parameters is to simulate the situation with 36 turbines at the end of Subsection 5-2-1. This situation is sensitive only in the parameters that depend on the turbulence intensity and thereby control the downwind wake velocity deficit in a one-turbine case. It is possible to check that the power fit at 10D can be improved by tuning these parameters by simply handtuning one. This is done in Figure 5-9.

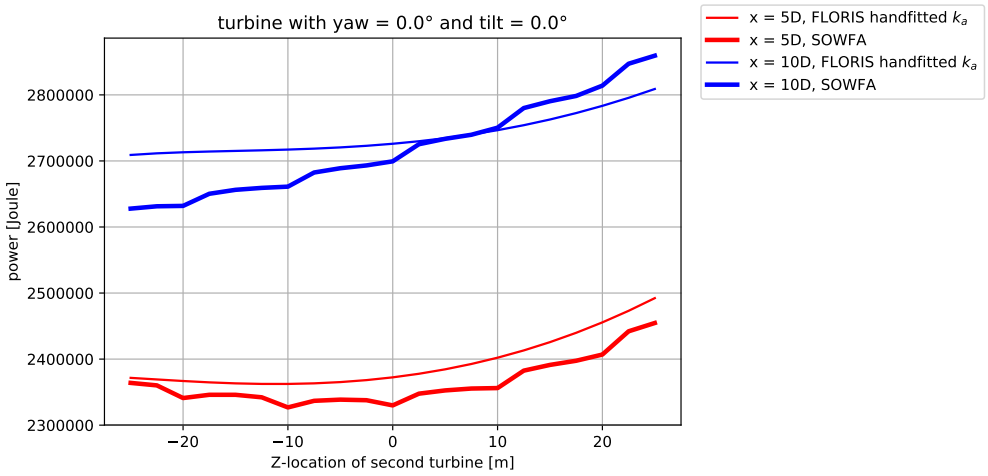

Figure 5-9: Power production of two turbines with second turbine at $\Delta x = [5D, 10D]$ and $\Delta z = [-25 : 2 : 25]$. New handfitted expansions parameter k_a

5-3 Conclusion

A general problem in any model fitting context is overfitting. The two usual solutions, reducing model complexity and gathering more data, are only partly applicable. By tuning on flow data instead of power data the CFD simulations become more valuable since more of their data is used for tuning. Reducing the model complexity is also not a viable approach since the model is already as simplified as possible. However, we can find situations where some of the parameters account for most of the models sensitivity. These specific situations can than be used to tune the relevant sensitive parameters. This is in many ways similar to formulating a reduced order model.

Chapter 6

Case Study

The previous chapters detailed how the FLOw Redirection and Induction in Steady state (FLORIS) model works and how it was modified to include the effects of turbine tilting. In this chapter, a case study will be performed using Computational Fluid Dynamics (CFD) software to test if the extended FLORIS model can be used to optimize the power production of a wind farm. This case study will be a similar to the case study detailed in [Gebraad et al., 2014].

There are two big differences between that case study and the case study in this chapter. Instead of the zoned wake model, explained in section 3-1, we will switch to the Porté-Agel model, explained in Section 3-2, which has a stronger theoretical foundation. The rotor tilt extension as explained in Section 4-2 will be tested as well. The case study in this thesis includes a baseline simulation with greedy control settings, a simulation with optimized yaw angles, a simulation where the tilt angles are optimized and a case where both the yaw and tilt angles are optimized simultaneously. The blade pitch angles are kept at zero degrees in all cases.

6-1 CFD packages

In this section the two CFD packages used in this casestudy are shortly described. The first is the Simulator for Onshore/Offshore Wind Farm Applications (SOWFA) and the second package is called the PArallelized LES Model (PALM).

On the website of the National Renewable Energy Laboratory (NREL) a short description of SOWFA is given [M. Churchfield, 2015], it is quoted here:

" *SOWFA is a set of CFD solvers, boundary conditions, and turbine models based on the OpenFOAM CFD toolbox. It includes a version of the turbine model coupled with Fatigue, Aerodynamics, Structures and Turbulence (FAST). This tool allows users to investigate wind turbine and wind plant performance under the full range of atmospheric conditions and in terrain.*

The package includes:

- *Atmospheric Boundary Layer (ABL) solver*
- *Wind plant solver*
- *Actuator line turbine model class (standard and coupled with FAST)*
- *Atmospheric/wind plant specific boundary condition classes*
- *Utilities for flow field initialization*
- *Utility to convert precurson sampled boundary data to inflow data for wind plant solver*

”

There are several different ways to model a wind farm in SOWFA. In this case study the Actuator Disk Model with Rotation (ADMR) will be used to model wind turbines. ADMR refers to an implementation of an actuator disk which is split up in sectors. The force applied by each sector on the flow is an approximation of a wind turbine.

PALM is likewise a CFD package that models the boundary layer of the atmosphere. It does not contain an equivalent to the FAST package but since this thesis is not focused on turbine loading that is not a problem. Palm will use its implementation of ADMR to run the case study.

6-2 Layout

The model turbine is the NREL5MW turbine with a rotor diameter of 126m [Jonkman et al., 2009]. the FLORIS model needs static mappings from the turbine control settings to the non-dimensionalized thrust coefficient, C_T, and power coefficient, C_P. This mapping is implemented as a Look Up Table (LUT) which is based on aero-elastic simulations with the FAST aero-elastic turbine model. These values are computed by running the simulations under quasi-static inflow conditions for a certain duration until a quasi steady state forms. From that point forward, the power and thrust coefficient are time-averaged and stored in the LUT as a function of windspeed and blade pitch. Conforming to the case study from [Gebraad et al., 2014], an atmospheric turbulence intensity, I_0, of 6% will be used, resulting in the near wake length as defined in (3-12) is 564m at this I_0. A turbine spacing of 5D will be used in the case study.

We will only be investigating the wind aligned case. This means that the cross wind spacing can be small, we chose a spacing of 3D. The wind-aligned case is the most crucial for wake-losses, which makes it a logical first step in comparing the effectiveness of tilt- and yaw-control.

6-3 Optimization

To optimize the control settings, a Sequential Least SQuares Programming (SLSQP) routine will be used to maximize the total power production. The SLSQP implementation found in the SciPy software library [Jones et al., 01] is used for optimization. The value function is the total power production. The absolute tolerance on the final result is 1×10^{-2}[W]. The tolerance on the jacobian is set to: 5×10^{-1}[W/rad]. No optimization boundaries are used.

This optimization procedure will find a local optimum from its starting point. Since the cost function is not convex, there is no guaranteed method for finding the global maximum. The

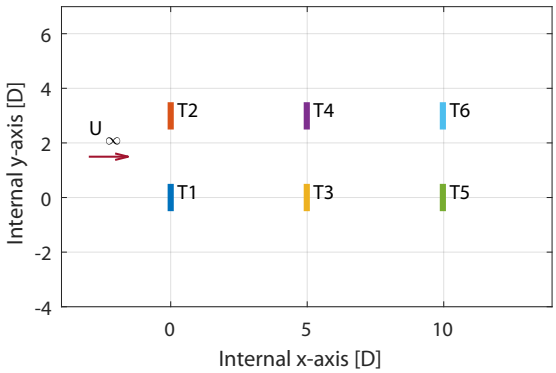

Figure 6-1: layout of the case study

non-convexity of the cost function is apparent from the fact that both positive and negative yaw angles lead to a power increase in the wind aligned case. Three different scenarios were investigated. In the first scenario only the tilt angles are optimized, in the second case both the tilt and yaw angles are optimized simultaneously, and in the third case only the yaw angles are optimized. The results of these optimizations are shown in Table 6-1. The greedy simulation case is included as the baseline case. In all the simulation cases, the turbines have a collective blade pitch angle of 0°.

Table 6-1: predicted power production of optimized cases by the FLORIS model and their required control settings

		Turb. 1	Turb. 2	Turb. 3	Turb. 4	Turb. 5	Turb. 6
baseline	yaw [°]	0	0	0	0	0	0
	tilt [°]	0	0	0	0	0	0
P = 7.71 MW	P[MW]	1.84	1.84	0.66	0.66	1.36	1.36
tilt	yaw [°]	0	0	0	0	0	0
	tilt [°]	24.92	24.92	0.25	0.23	-0.82	-0.33
P = 8.48 MW	ΔP[MW]	-0.34	-0.34	0.62	0.62	0.10	0.10
yaw & tilt	yaw [°]	17.18	17.89	3.87	3.87	-0.16	-0.16
	tilt [°]	17.24	17.27	0.94	0.96	-0.45	-0.45
P = 8.64 MW	ΔP[MW]	-0.30	-0.32	0.67	0.68	0.10	0.09
yaw	yaw [°]	23.01	23.01	3.45	3.45	-1.92	-1.92
	tilt [°]	0	0	0	0	0	0
P = 8.61 MW	ΔP[MW]	-0.27	-0.27	0.65	0.65	0.06	0.06

The turbine numbering starts at the first column of turbines and ends at the last, e.g., turbines 1, 3 and 5 form one row. The turbine rows are defined as being along the the streamwise axis. The table shows that the FLORIS model predicts the largest gains to occur by misaligning the two upstream rotors, namely turbine one and two. The other four turbines are predicted to require only small yaw and tilt angles. Consequently, most of the power increase happens on the second turbine column, with turbine three and four approximately doubling in output in each optimized case.

6-4 High-fidelity simulation results

The optimal control settings shown in Table 6-1 are implemented in two large scale CFD packages to investigate if the predicted power increases also occur here. The two packages, the PALM and the SOWFA, are both Large Eddy Simulation (LES) programs. Both programs ran a simulation of 1000 seconds at the control settings shown in Table 6-1. To start analyzing the results we will average the flowfields from 300-1000 seconds at hub height and simply plot them. The first 300 seconds are omitted because the wakes are still forming in this time period. The time-averaged flowfields are shown in Figure 6-2. The plot contains the baseline, and optimized simulations from left to right. The results of SOWFA are in the first row, the PALM results in the second row and the FLORIS prediction is at the bottom. The powers are listed in Table 6-2 and discussed after the flows are discussed.

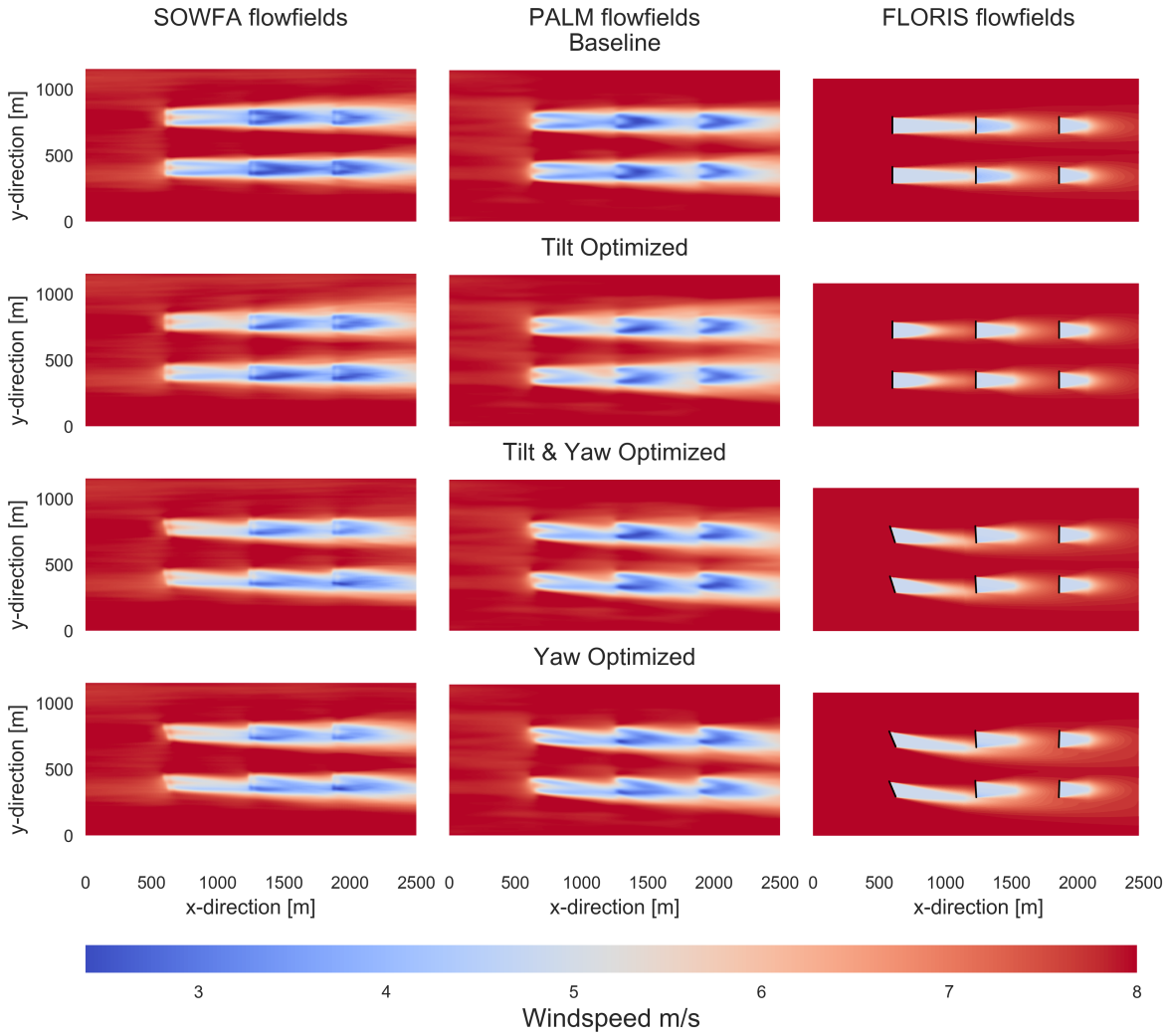

Figure 6-2: Hub height time averaged velocity field as predicted by SOWFA, PALM and FLORIS

One aspect the jumps out is that FLORIS predicts the second wake to be shorter than both PALM and SOWFA in every case. Properly fitting the added turbulence parameters might decrease this mismatch. However due to time-restrictions this will be relegated to future

work. Section 5-2 details a proposal to accurately tune the relevant parameters. Both the near-wake length parameters, α and β, and the wake expansion parameters, k_a and k_b, are modulated by the local total turbulence intensity, I. On first glance it seems that in each of the simulated cases, I is too high at the second rotor, causing a wake that is both too short and decays too quickly. The first rotor adds turbulence to the flow hitting the second rotor. The added turbulence model has four fitting parameters, I_a, I_b, I_c and I_d. These are probably the main drivers for the difference in length of the second wake observed between the FLORIS model and the CFD results in Figure 6-2.

Since we are interested in the tilting behaviour, we will also look at a time-averaged flow field slice through the first row. This is shown in Figure 6-3.

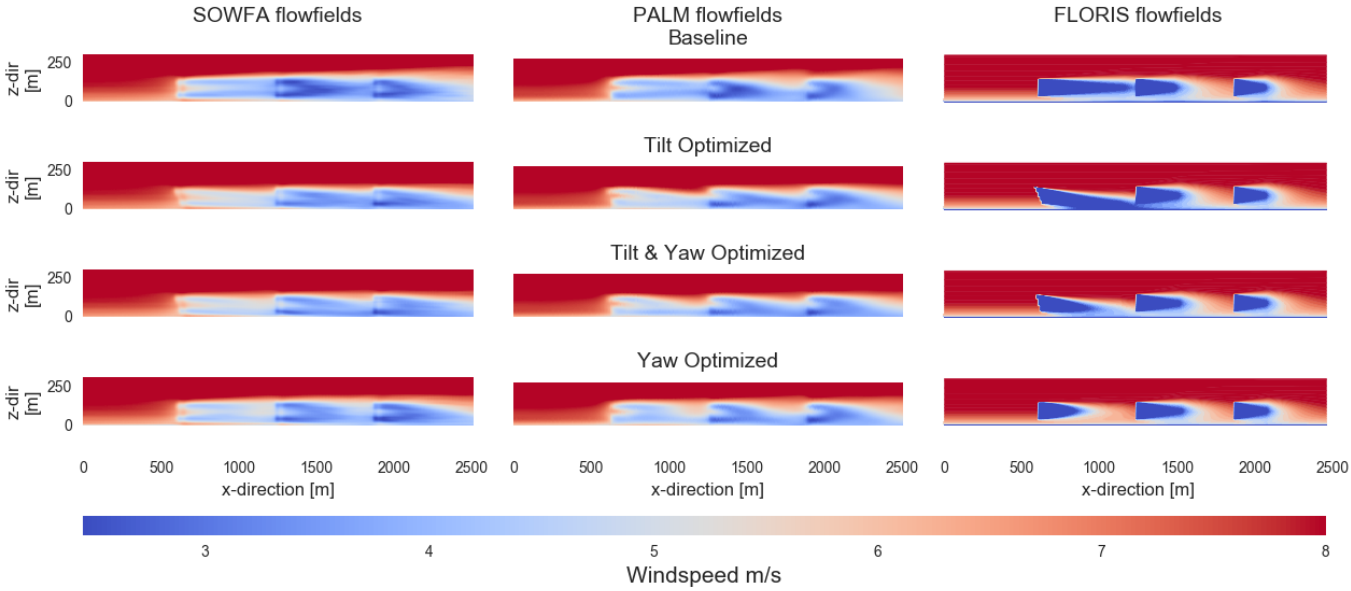

Figure 6-3: First row time averaged velocity field as predicted by SOWFA, PALM and FLORIS

An interesting observation is that the wake of the first turbine in the tilted case seems to disappear into the ground in the FLORIS model. This does not happen in PALM and SOWFA. The power gains realized in the CFD simulations are probably less than those estimated by FLORIS because of this effect.

We start investigating the produced power in SOWFA and PALM by plotting the power time series for each turbine in the first row. The turbines in the second row behave largely similar and are omitted for this reason. The mean power production from 300 until 1000 seconds is computed for each turbine for each case and plotted as well. This is shown in Figure 6-4 for SOWFA and in Figure 6-5 for PALM.

The bar graphs in the subaxes on the right shows how the time-averaged power of each case stacks up against the power as predicted by FLORIS for that turbine and case. The results generated by both SOWFA and PALM are similar, but PALM predicts slightly more power than SOWFA. FLORIS under-predicts the amount of power generated in the first turbine and over-predicts the amount of power on the last turbine. In the second turbine, there is also a small but consistent over prediction, i.e., the time-averaged turbine power capture predicted by FLORIS is higher than that predicted by the high-fidelity simulation models.

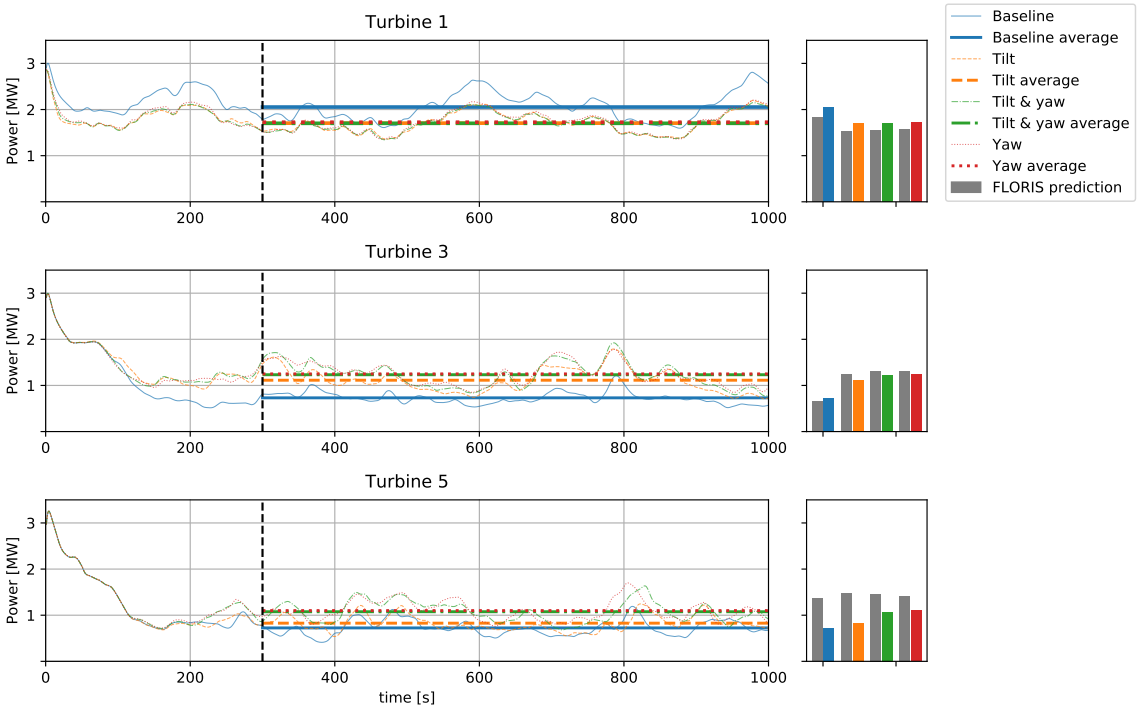

Figure 6-4: Power production of the first turbine row in SOWFA

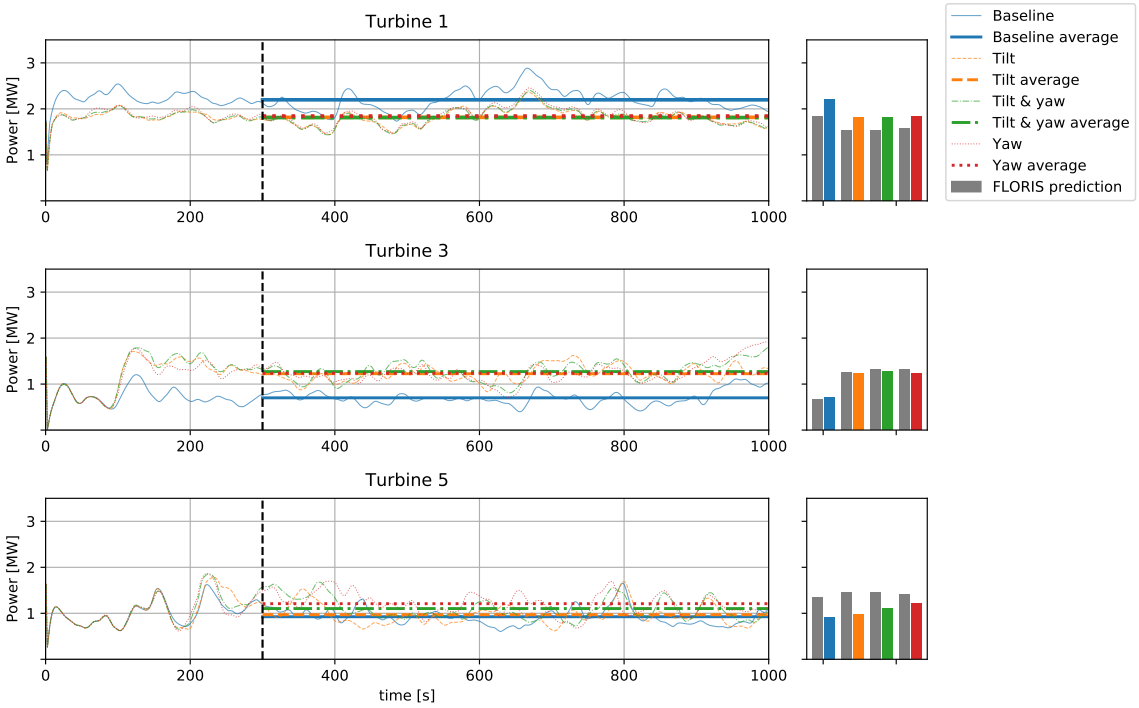

Figure 6-5: Power production of the first turbine row in PALM

Figure 6-4 and Figure 6-5 show quite clearly how the power predictions vary from turbine to turbine and how the predictions from FLORIS differ from those from the CFD packages. As was seen in Figure 6-2, FLORIS underestimates the length of the second wake leading to an overestimation of the power prediction in the last turbine column.

Figure 6-6 shows how the total power production changes in the three optimized cases. The total power captured by the wind farm is also tabulated in Table 6-2. The first thing to notice is that FLORIS overestimates the power production in every case. The overestimation is largest in the case where only the tilt angles are optimized. This is probably due to the aforementioned 'missing ground effect' in FLORIS. In FLORIS, there is currently no mechanism to model the ground. This means that the wake can simply continue into negative z-values, i.e., the wake exists below the ground.

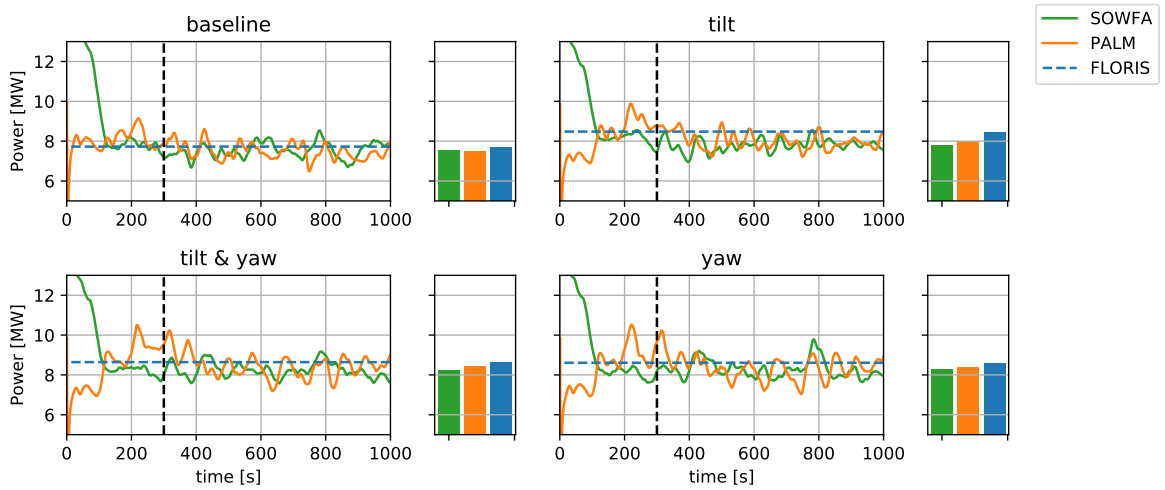

Figure 6-6: Power production of the first turbine row in PALM

Table 6-2: Total time-averaged power generation as graphed in Figure 6-6

	SOWFA		PALM		FLORIS	
Baseline Power [MW]	7.53	-	7.50	-	7.71	-
Tilt Power [MW]	7.80	+3.59 %	8.02	+6.93 %	8.48	+9.99 %
Tilt & Yaw Power [MW]	8.25	+9.56 %	8.46	+12.80 %	8.64	+12.06 %
Yaw Power [MW]	8.29	+10.09 %	8.36	+11.47 %	8.61	+11.67 %

6-5 Conclusion

The power gains predicted by FLORIS are optimistic. FLORIS underestimates the wake length of turbines that experience added turbulence from upwind turbines. In this case study that effect causes the last column of turbines to have an unrealistically high power production according to LES simulations. This can possibly be alleviated by better tuning of the added turbulence model as described in Section 5-2.

Currently FLORIS does not have any way to model the effect of the ground on wakes which leads to a large overprediction of power production when the control settings are only optimized for tilt. In plume modelling, a widely used method to model the ground in low-order models is to implement a virtual second copy of the plume below the ground [Kenneth Wark, 1997]. Then, when the original plume goes below the ground, it's mirror image functions as if the ground is reflecting the plume. Maybe a similar tactic can be employed in the FLORIS model.

Chapter 7

Conclusions

The objectives of this thesis consisted of:

1. Implement the effects of rotor tilting on the wake and turbine power production in a reduced order model
2. Investigate the validity of the model and tune the model to high fidelity simulations
3. Perform a case study in which the total power yield of a small wind farm is optimized using turbine tilt
4. Program the new extension in such a way that the model is modular and easily extendable. Open-source this model such that other people can make use of it.

These stated objectives have been partially reached. The previous deflection models, described in [Jiménez et al., 2009] and [Bastankhah and Porté-Agel, 2016], constructed a relationship between the yaw angle, the drop in rotor power capture and the wake deflection. To investigate the effects of rotor tilting this mechanism was extended in the following way:

1. yaw is modelled in a horizontal plane and causes lateral deflection.
2. Tilt relies on the same principle but in a vertical plane.
3. To combine both, a rotated plane is identified by computing the angle between the turbine thrust and the turbine inflow wind direction. This is called the thrust angle.
4. The wake deflection happens in the rotated plane

Implementing rotor tilting has two effects on FLOw Redirection and Induction in Steady state (FLORIS). The first is that any misalignment between the rotor thrust and the mean inflow wind direction causes a drop in rotor power capture. The second effect is that the downstream wake can be deflected out of the horizontal plane that intersects the turbine hub.

One of the main advantages of implementing rotor tilting in this manner is that it does not require any additional fitting parameters. However, the original wake deflection models assume a uniform inflow, this assumption is not entirely valid along the vertical axis. Whether

this poses a big problem will need to be investigated further. Before it is possible to determine how big the errors are, the extended model should be tuned. To start this investigation, a sensitivity analysis was performed. This sensitivity analysis formed the basis for a proposed fitting scheme for the tunable model parameters. However, due to lack of computational resources and lack of time, this fitting was not completed. In the end, only the turbine rotation induced vertical wake deflection parameters, a_T and b_T, were tuned. The other parameters where kept at their original nominal parameters.

With the extended and partially tuned model, a case study was performed. The case study was a simulation of a small wind farm with six wind turbines in a 2x3 layout. The model was used to identify optimal control settings using rotor tilt, rotor tilt & yaw, or only rotor yaw. The case study showed that FLORIS consistently over predicted the amount of power that could be gained with different control settings. Two different effects seems to cause most of the disagreement between the Large Eddy Simulation (LES) programs and FLORIS. The first reason is that the wake length of rotors that are downwind of other turbines is underestimated by FLORIS. This causes an overestimation in the power production of turbines that are third in a row. The second reason is that currently FLORIS has no method of modeling the effect of the ground on a wake. This means that in the FLORIS model it is possible to deflect a wake into the ground. In the LES programs the wake will stay above the surface and affect downwind rotors.

Despite this effect, the case where both the yaw and tilt angles of the rotor where optimized simultaneously showed a large improvement in power production. The FLORIS model predicted an increase of 12.1% and Simulator for Onshore/Offshore Wind Farm Applications (SOWFA) and PArallelized LES Model (PALM) predicted 9.6% and 12.8% respectively. The yaw angles in this case were 30% smaller than in the case where only the yaw angles were optimized. Since both LES packages show sizable increase in power extraction this bodes well for control strategies combining rotor yaw and tilt.

7-1 Recommendations

A number of recommendations can be made for this thesis.

The wake deflection models rely on the assumption of uniform flow. The effect of the non-uniform flow in an atmospheric boundary layer on wake deflection should be further investigated. It would be interesting to quantify this and correct for it in FLORIS.

The effect of rotor misalignment on the thrust and power coefficent is also worth investigating. In the literature on yaw misalignment, each researcher seems to apply these metrics in a different way. There is no systematic investigation between the relationship proposed by Actuator Disk Model (ADM) and how it holds up under misaligned rotor conditions.

Furthermore, the tuning procedure as outlined in Chapter 5 should be completed. This might solve the problem of under prediction of the wake length. Either way, it will yield confidence intervals on the tuning parameters.

Finally, FLORIS should be extended to model ground effects. One idea could be to model a copy of each turbine mirrored with respect to the ground. This effectively creates a mirror image of each wake and lets the ground reflect each wake.

Bibliography

[Annoni et al., 2016] Annoni, J., Gebraad, P. M. O., Scholbrock, A. K., Fleming, P. A., and van Wingerden, J.-W. (2016). Analysis of axial-induction-based wind plant control using an engineering and a high-order wind plant model. *Wind Energy*, 19(6):1135–1150.

[Annoni et al., 2017] Annoni, J., Scholbrock, A., Churchfield, M., and Fleming, P. (2017). Evaluating Tilt Control for Wind Farms.

[Annoni et al., 2014] Annoni, J., Seiler, P., Johnson, K., Fleming, P., and Gebraad, P. (2014). Evaluating wake models for wind farm control. *Proceedings of the American Control Conference*, pages 2517–2523.

[Bastankhah and Porté-Agel, 2014] Bastankhah, M. and Porté-Agel, F. (2014). A new analytical model for wind-turbine wakes. *Renewable Energy*, 70:116–123.

[Bastankhah and Porté-Agel, 2016] Bastankhah, M. and Porté-Agel, F. (2016). Experimental and theoretical study of windturbine wakes in yawed conditions. *Journal of Fluid Mechanics*, 806:506–541.

[Beiter et al., 2017] Beiter, P., Musial, W., Kilcher, L., Maness, M., Smith, A., Beiter, P., Musial, W., Kilcher, L., Maness, M., and Smith, A. (2017). An Assessment of the Economic Potential of Offshore Wind in the United States from 2015 to 2030 An Assessment of the Economic Potential of Offshore Wind in the United States from 2015 to 2030. (March).

[Betz, 1926] Betz, A. (1926). *Wind-energie und ihre ausnutzung durch windmühlen*. Vandenhoeck.

[Bianchi et al., 2007] Bianchi, F. D., Battista, H. d., and Mantz, R. J. (2007). *Wind Turbine Control Systems*. springer.

[Boersma et al., 2016] Boersma, S., Doekemeijer, B. M., Gebraad, P. M. O., Fleming, P. A., Annoni, J., Scholbrock, A. K., Frederik, J. A., and Wingerden, J. W. V. (2016). A Tutorial on Control-Oriented Modeling and Control of Wind Farms.

[Campagnolo et al., 2016] Campagnolo, F., Petrović, V., Schreiber, J., Nanos, E. M., Croce, A., and Bottasso, C. L. (2016). Wind tunnel testing of a closed-loop wake deflection controller for wind farm power maximization. *Journal of Physics: Conference Series*, 753(3).

[Charhouni et al., 2015] Charhouni, N., Arbaoui, A., and Sallaou, M. (2015). Qualification of three analytical wake models. *22ème Congrès Français de Mécanique*.

[Crespo and Hernández, 1996] Crespo, A. and Hernández, J. (1996). Turbulence characteristics in wind-turbine wakes. *Journal of Wind Engineering and Industrial Aerodynamics*, 61(1):71–85.

[Fleming et al., 2015] Fleming, P., Gebraad, P. M. O., Lee, S., Van Wingerden, J. W., Johnson, K., Churchfield, M., Michalakes, J., Spalart, P., and Moriarty, P. (2015). Simulation comparison of wake mitigation control strategies for a two-turbine case. *Wind Energy*, 18(12):2135–2143.

[Fleming et al., 2014] Fleming, P. A., Gebraad, P. M. O., Lee, S., van Wingerden, J. W., Johnson, K., Churchfield, M., Michalakes, J., Spalart, P., and Moriarty, P. (2014). Evaluating techniques for redirecting turbine wakes using SOWFA. *Renewable Energy*, 70:211–218.

[Gebraad et al., 2017] Gebraad, P., Thomas, J. J., Ning, A., Fleming, P., and Dykes, K. (2017). Maximization of the annual energy production of wind power plants by optimization of layout and yaw-based wake control. *Wind Energy*, 20(1):97–107.

[Gebraad et al., 2014] Gebraad, P. M. O., Teeuwisse, F. W., Van Wingerden, J. W., Fleming, P. A., Ruben, S. D., Marden, J. R., and Pao, L. Y. (2014). A data-driven model for wind plant power optimization by yaw control. *Proceedings of the American Control Conference*, pages 3128–3134.

[Gebraad et al., 2016] Gebraad, P. M. O., Teeuwisse, F. W., Van Wingerden, J. W., Fleming, P. A., Ruben, S. D., Marden, J. R., and Pao, L. Y. (2016). Wind plant power optimization through yaw control using a parametric model for wake effects - A CFD simulation study. *Wind Energy*, 19(1):95–114.

[Gebraad and Wingerden, 2015] Gebraad, P. M. O. and Wingerden, J. W. (2015). Maximum power-point tracking control for wind farms. *Wind Energy*, 8:429–447.

[Göçmen and Giebel, 2016] Göçmen, T. and Giebel, G. (2016). Estimation of turbulence intensity using rotor effective wind speed in Lillgrund and Horns Rev-I offshore wind farms. *Renewable Energy*, 99:524–532.

[Jensen, 1983] Jensen, N. O. (1983). A note on wind generator interaction. *Risø-M-2411 Risø National Laboratory Roskilde*, pages 1–16.

[Jiménez et al., 2009] Jiménez, Á., Crespo, A., and Migoya, E. (2009). Application of a LES technique to characterize the wake deflection of a wind turbine in yaw. *Wind Energy*, 13(6):559–572.

[Johnson, 2004] Johnson, K. E. (2004). Adaptive Torque Control of Variable Speed Wind Turbines. (August):107.

[Jones et al., 01] Jones, E., Oliphant, T., Peterson, P., et al. (2001–). SciPy: Open source scientific tools for Python. [Online; accessed ¡today¿].

[Jonkman et al., 2009] Jonkman, J., Butterfield, S., Musial, W., and Scott, G. (2009). Definition of a 5-MW Reference Wind Turbine for Offshore System Development. (February).

[Katic I., 1986] Katic I., Hojstrup J., J. N. O. (1986). A simple model for cluster efficiency i.katic. j.højstrup. n.o.jensen. *Ewea 1986*, (October):407–410.

[Kenneth Wark, 1997] Kenneth Wark, C. F. W. (1997). *Air Pollution: Its Origin and Control*. Pearson.

[Larsen, 1988] Larsen, G. (1988). A Simple Wake Calculation Procedure. *Risø-M*, No. 2760:58.

[Lee & Chu, 2003] Lee & Chu, Joseph Hun-wei Lee, V. C. (2003). springer.

[M. Churchfield, 2015] M. Churchfield, S. L. (2015). Nwtc information portal (sowfa). https://nwtc.nrel.gov/SOWFA.

[Machefaux et al., 2015] Machefaux, E., Larsen, G. C., and Leon, J. P. (2015). Engineering models for merging wakes in wind farm optimization applications. *Journal of Physics: Conference Series*, 625(1).

[Niayifar and Porté-Agel, 2015] Niayifar, A. and Porté-Agel, F. (2015). A new analytical model for wind farm power prediction. *Journal of Physics: Conference Series*, 625:012039.

[Rajaratnam, 1977] Rajaratnam, N. (1977). Turbulent jets. by n. rajaratnam. elsevier, 1976. 304 pp. 23.45. *Journal of Fluid Mechanics*, 82(3):607608.

[Thomas et al., 2016] Thomas, J. J., Gebraad, P. M. O., and Ning, A. (2016). Improving the FLORIS Wind Plant Model for Compatibility with Gradient-based Optimization. *Wind Engineering*, (In review):1–16.

[van Dijk et al., 2016] van Dijk, M. T., van Wingerden, J.-W., Ashuri, T., Li, Y., and Rotea, M. A. (2016). Yaw-Misalignment and its Impact on Wind Turbine Loads and Wind Farm Power Output. *Journal of Physics: Conference Series*, 753:062013.